JGR Oceans

RESEARCH ARTICLE
10.1029/2025JC022330

# Sea-Ice Retreat by Eddies in the Marginal Ice Zone of the East Greenland Current

**Igor L. Bashmachnikov[1,2,3], Sergey S. Pryakhin[4], Igor E. Kozlov[3], Claudia Wekerle[5], Wenli Zhong[6,7], Sergey A. Shliapin[1], and Anastasiia S. Kaledina[1,2]**

[1]Department of Oceanography, St. Petersburg State University, St. Petersburg, Russian Federation, [2]Nansen International Environmental and Remote Sensing Centre, St. Petersburg, Russian Federation, [3]Marine Hydrophysical Institute of RAS, Sevastopol, Russian Federation, [4]Arctic and Antarctic Research Institute, St. Petersburg, Russian Federation, [5]Physical Oceanography, Alfred Wegener Institute, Helmholtz Centre for Polar and Marine Research, Bremerhaven, Germany, [6]Frontier Science Center for Deep Ocean Multispheres and Earth System (FDOMES) and Physical Oceanography Laboratory, Ocean University of China, Qingdao, China, [7]Laoshan Laboratory, Qingdao, China

**Abstract** This study aims to investigate the effect of eddies on synoptic variability of the sea-ice edge along the East Greenland Current (EGC) in the northwestern Greenland Sea. We use an eddy-resolving FESOM1.4 ocean model configuration with 1 km spatial resolution in the Fram Strait. The synoptic variations of the sea-ice area in the region proved to be a result of an interplay between the regional convergence of the sea-ice advected from the Arctic and a local sea-ice freezing or melting. Several case studies showed that eddies in the marginal ice zone (MIZ) can effectively decrease the ice area, resulting in a local retreat of the ice-edge by 3–8 km per day. However, these local retreats of the MIZ in the Greenland Sea are quickly restored by an enhanced convergence of the advected ice or, during the cold period, by atmospheric cooling, keeping the monthly mean MIZ position stable in time. The integral effect of eddies on the ice extent is to limit the ice spreading east from the EGC. The effect of the eddies resides on strong regional temperature gradients east of the MIZ formed by the convergence of the cold Polar Water with warm Recirculating Atlantic Water.

**Plain Language Summary** Ocean mesoscale eddies are the most important agent of horizontal mixing across oceanic fronts, reducing the gradients of water characteristics. It is assumed that eddies can also be an important factor of the sea-ice retreat of the sea-ice margin, especially in the regions, where sea-surface temperature gradients are large. One of such areas is the northern Greenland Sea, where a strong sea-ice discharge from the Arctic meets with the warmer Atlantic water inflow coming from the south. In this study the effect of eddies on the Marginal Ice Zone (MIZ) in the East Greenland Current (EGC) is studied using an eddy-resolving FESOM1.4 ocean model with 1 km spatial resolution. It is found that the horizontal mixing with ocean eddies can effectively decrease the ice area, resulting in a local retreat of the ice-edge by 3–8 km per day. However, such retreats are quickly restored. The counterbalance between the sea-ice convergence due to advection of the sea-ice with the EGC and the ice melt due to horizontal eddy mixing makes the MIZ stable during most of the year.

**Key Points:**

- Eddies can effectively decrease the sea-ice area, resulting in a local retreat of the ice-edge by 3–8 km per day
- The horizontal eddy heat flux of 1TW in the northern Greenland Sea is sufficient to balance the local sea-ice convergence by advection
- The integral effect of eddies on the ice extent is to limit the ice spreading east from the East Greenland Current

**Supporting Information:**

Supporting Information may be found in the online version of this article.

**Correspondence to:**

I. L. Bashmachnikov,
igorb1969@mail.ru

**Citation:**

Bashmachnikov, I. L., Pryakhin, S. S., Kozlov, I. E., Wekerle, C., Zhong, W., Shliapin, S. A., & Kaledina, A. S. (2025). Sea-ice retreat by eddies in the marginal ice zone of the East Greenland Current. *Journal of Geophysical Research: Oceans*, *130*, e2025JC022330. https://doi.org/10.1029/2025JC022330

Received 6 JAN 2025
Accepted 30 OCT 2025

**Author Contributions:**

**Conceptualization:** Igor L. Bashmachnikov
**Data curation:** Sergey S. Pryakhin, Igor E. Kozlov, Claudia Wekerle
**Formal analysis:** Igor L. Bashmachnikov, Sergey S. Pryakhin, Igor E. Kozlov, Claudia Wekerle, Wenli Zhong, Sergey A. Shliapin, Anastasiia S. Kaledina
**Funding acquisition:** Igor E. Kozlov, Wenli Zhong
**Investigation:** Igor L. Bashmachnikov, Sergey S. Pryakhin, Igor E. Kozlov, Claudia Wekerle, Wenli Zhong, Sergey A. Shliapin, Anastasiia S. Kaledina
**Methodology:** Igor L. Bashmachnikov
**Project administration:** Igor E. Kozlov
**Resources:** Igor E. Kozlov, Claudia Wekerle
**Software:** Sergey S. Pryakhin, Claudia Wekerle, Sergey A. Shliapin, Anastasiia S. Kaledina
**Supervision:** Igor L. Bashmachnikov, Igor E. Kozlov



## 1. Introduction

The Greenland Sea is one of the key regions of deep ocean convection, an inherent part of the Atlantic Meridional Overturning Circulation (Buckley & Marshall, 2016; Rhein et al., 2011). Interannual variations in the intensity of deep convection, in turn, are primarily governed by oceanic buoyancy advection in the sea, while ocean-atmosphere heat and freshwater exchange play a secondary role in this region (Bashmachnikov et al., 2021; Kaledina & Bashmachnikov, 2023). The freshwater advection plays the principal role in the long-term buoyancy balance of the upper Greenland Sea (Alekseev et al., 2001; Meincke et al., 1992). The precipitation-evaporation difference is positive, but accounts only for 15% of the freshwater balance, while approximately a half of the temporal variations of the freshwater in the Norwegian-Greenland region are due to the freshwater flux through the Fram Strait. This includes the waters of Arctic origin (the Polar Water, PW) and the sea-ice transport (Glessmer et al., 2014; Peterson et al., 2006; Serreze et al., 2006).

The sea-ice extent in the Greenland Sea is highly variable (Germe et al., 2011). Around 80% of the sea-ice comes from the Arctic (Mironov, 2004). This sea-ice flux is primarily controlled by regional atmospheric circulation patterns (Kwok, 2004; Ricker et al., 2018; Vinje & Finnekåsa, 1986). Thus, with the positive phase of the Arctic

**Validation:** Igor L. Bashmachnikov, Igor E. Kozlov, Wenli Zhong
**Visualization:** Sergey S. Pryakhin, Sergey A. Shliapin, Anastasiia S. Kaledina
**Writing – original draft:** Igor L. Bashmachnikov, Sergey S. Pryakhin
**Writing – review & editing:** Igor L. Bashmachnikov, Igor E. Kozlov, Claudia Wekerle, Wenli Zhong

Oscillation, or of its regional counterpart—the North Atlantic Oscillation, the northerly winds in the northwestern Greenland Sea increase a sea-ice transport through the Fram Strait (Kwok, 2004; Marshall et al., 2001). Besides the Arctic ice, winter conditions allow for local sea-ice production in the Greenland Sea. North of 70°N the highest interannual variations of the sea-ice area is linked to local sea-ice formation (Germe et al., 2011). In the southern part of the Greenland Basin, the variability of the sea-ice area is primarily due to an occasional formation of the Odden ice tongue, a pattern extending from the Greenland shelf to northwest of Jan Mayen (Comiso et al., 2001; Wadhams et al., 1996). A decrease in the intensity of the northerly winds and their change to southerly winds favors a larger Odden tongue (Germe et al., 2011; Shuchman et al., 1998). Therefore, the Odden tongue area strongly negatively (−0.7) correlates with air temperatures near Jan Mayen (Comiso et al., 2001).

In the annual mean, about 90% of the sea-ice advected from the Arctic across the Fram Strait melts in the Greenland Sea (Selyuzhenok et al., 2020). This decreases the upper ocean salinity in the East Greenland Current (EGC) and sharpens the EGC front. Decadal peaks in the sea-ice transport through the Fram Strait are thought to give rise to the Great Salinity anomalies in the North Atlantic (Haak et al., 2003) that penetrate further south and can affect the deep convection in the Subpolar Gyre (Dukhovskoy et al., 2019).

The long-term tendencies in the area and volume of the sea-ice in the Greenland Sea are associated with an increase in the sea-surface water temperature, which is a result of a penetration of the Recirculating Atlantic Water (RAW) into the Greenland Basin (Selyuzhenok et al., 2020). As the subsurface core of the RAW is observed at 200–700 m depth, vertical water exchange enhances the sea-ice melt. In particular, it is speculated that oceanic convection of intermediate intensity favors an intensification of the upward heat flux, affecting the air temperature and sea-ice extent (Comiso et al., 2001; Selyuzhenok et al., 2020; Visbeck et al., 1995). In the ice-covered EGC region, where the PW overlays the warmer RAW, warm-core anticyclonic eddies under the sea-ice can force a faster ice melt through upward Ekman pumping, which induces high upward velocities of 1–10 cm $s^{-1}$ sustained up to 1–2 days (Gupta et al., 2020). The vertical motions in the subsurface eddies (Bashmachnikov et al., 2018), tidal mixing and quasi-stationary vertical motions (Luneva et al., 2015) form other mechanisms for the RAW penetration in the upper mixed layer.

The formation of local sea-ice cover in the Greenland Sea begins in September. Freezing temperatures are initially reached in-between the sea-ice floes advected from the Arctic. The maximum sea-ice growth rate is reached in October-November. The ice formation continues until February-March, when the seasonal winter sea-ice area maximum in the Greenland Sea is registered, about 2 months earlier than that in other Eurasian Arctic seas (Mironov, 2004). The ice extent in the Greenland Sea remains relatively stable during March and April, when the positive radiation balance already compensates for the oceanic heat release to the atmosphere in the ocean/ice surface heat balance. From June the sea-ice area starts decreasing, reaching its seasonal minimum in August or September (Mironov, 2004).

Over the recent decades, despite an increase of the sea-ice area and volume flux in the Fram Strait, the winter sea-ice area in the Greenland Sea shows a gradual reduction (Kwok et al., 2004; Smedsrud et al., 2017; Widell et al., 2003). During this latter period the Odden ice tongue did not form (Germe et al., 2011; Rogers & Hung, 2008). This was due to an intensification of the ice melt, in particular, due to a stronger heat advection with the RAW from the West Spitsbergen Current in the Greenland Basin (Selyuzhenok et al., 2020). The confluence of the RAW with the PW along the EGC creates high sea-surface temperature (SST) and salinity gradients, in particular in the northern part of the Greenland Sea, where cross-frontal horizontal exchange together with the vertical mixing are important factors in the sea-ice melt in the Greenland Sea (Perovich et al., 1989; Rudels et al., 2012; von Appen et al., 2015).

Mesoscale and submesoscale eddies are thought to be the main agents of the cross-frontal exchange in the World Ocean, also active in the Arctic (Fine et al., 2018; Meneghello et al., 2018; Spall et al., 2008). Numerous case studies show a strong eddy activity in the marginal ice zone (MIZ) of the EGC (Wadhams & Squire, 1983; Johannessen, Johannessen, Svendsen, Shuchman, Manley, et al., 1987,Johannessen, Johannessen, Svendsen, Shuchman, Campbell, et al., 1987; Manley, 1987; Smith et al., 1991; Sandven et al., 1991; von Appen et al., 2018; Bashmachnikov et al., 2020; Petrenko & Kozlov, 2023; Watkins et al., 2023), where a higher number of eddies is detected compared to the surrounding areas (Bashmachnikov et al., 2020; Kozlov & Atadzhanova, 2022; Trodahl & Isachsen, 2018; Wekerle et al., 2020). During the periods of a relatively stable sea-ice margin, eddies are mostly observed seawards of the MIZ area, but the ice edge begins its westward retreat as the maximum number of eddies migrates toward the MIZ (Petrenko & Kozlov, 2023). In situ and satellite observations, primarily synthetic aperture

radar (SAR) measurements, showed that the eddy radii in this area cover a large range of scales, from 1 to 40 km, with the mean values between 10 and 30 km (Johannessen, Johannessen, Svendsen, Shuchman, Manley, et al., 1987, Johannessen, Johannessen, Svendsen, Shuchman, Campbell, et al., 1987; Manley, 1987; Bondevik, 2011; Kozlov et al., 2020; Bashmachnikov et al., 2020; Kozlov & Atadzhanova, 2022). The detected azimuthal velocities in the eddy cores are high, ranging from 10 to 40 cm $s^{-1}$ and, at times, exceeding 60 cm $s^{-1}$ (Kozlov et al., 2020). Eddy translation velocities in the study region are typically in the range of 1–5 cm $s^{-1}$ (Bashmachnikov et al., 2020; Bondevik, 2011; Morozov & Kozlov, 2023). Short eddy tracks in the Fram Strait (on average 35 km) suggest local eddy generation (Wekerle et al., 2020).

Eddies in the EGC are thought to be generated by baroclinic and/or barotropic instability in the frontal zone of the EGC (Manucharyan & Timmermans, 2013; Trodahl & Isachsen, 2018). The baroclinic instability forms eddy dipoles in the EGC front, often observed in satellite data, about 20% of which leave the MIZ transporting sea-ice into the warmer waters (Manucharyan & Timmermans, 2013). Bottom topographic features are another source of eddy formation in the EGC (Bourke et al., 1987; Johannessen, Johannessen, Svendsen, Shuchman, Campbell, et al., 1987). Upwelling/downwelling motions in the MIZ are forced by a wind stress difference, as the air-ice momentum flux is, on average, 3 times greater than that translated to the open water (Häkkinen, 1986). The vertical motions at the MIZ form fronts which often become unstable. Downwelling fronts (formed in the study region during the southwesterly winds) are considered to be more unstable than the upwelling ones (the northeasterly winds in the study region) (Häkkinen, 1986).

The general direction of eddy drift is from the West Spitsbergen Current toward the EGC (Bashmachnikov et al., 2020; Wekerle et al., 2020), which is an important source of the regional heat convergence. In situ observations suggest that a significant fraction of the Atlantic Water of the West Spitsbergen Current is translated to the EGC by eddy flux (Boyd & D'Asaro, 1994; Nilsen et al., 2006; von Appen et al., 2016; Hattermann et al., 2016; Wekerle et al., 2017). Approaching the Polar Front, eddies induce an additional instability of the EGC (Smith et al., 1991). The generated cyclones get trapped by the EGC, while anticyclones generate coupled cyclones to form eddy dipoles that are further expelled from the EGC.

Eddies horizontally mix the warmer RAW and colder PW across the MIZ, as well as trap ice and translate it away from the MIZ. Most of eddies observed in the MIZ of the EGC in SAR and optical data are cyclonic (Bondevik, 2011; Kozlov & Atadzhanova, 2022; Morozov & Kozlov, 2023; Petrenko & Kozlov, 2023), however this may be biased by an easier identification of cyclones in SAR data (see discussion in Bashmachnikov et al., 2020). Ocean model studies suggest that ageostrophic ice convergence is observed predominantly in the centers of cyclones, which make them clearly visible in SAR and optical data, while anticyclones expel the ice (Manucharyan & Thompson, 2017). Recent SAR observations confirmed that cyclones trap more sea-ice than anticyclones, yet, the difference was not significant (Kozlov & Atadzhanova, 2022). Hence, more intense ice transport away from the MIZ is expected to be caused by cyclones, or when they couple with anticyclones in dipole structures. Ice may also be translated in filaments, which end in cyclonic or dipolar structures (von Appen et al., 2018; Kozlov et al., 2020).

The mesoscale and submesoscale eddies increase the horizontal turbulent diffusivity in the MIZ by orders of magnitude (Fine et al., 2018; Mensa et al., 2018; Pnyushkov et al., 2018). The eddy heat flux regionally can be comparable with the heat advection of the EGC (Manley, 1987). Early estimates suggest that eddies can force an ice edge retreat by 1–2 km per day (Johannessen, Johannessen, Svendsen, Shuchman, Campbell, et al., 1987), however more recent estimates indicate a more modest effect of around 0.5 km per day (Kozlov & Atadzhanova, 2022). In submesoscale eddies an upward heat flux to the ice base can also be important and reach in its extreme values 100 W $m^{-2}$ (Manucharyan & Thompson, 2017).

Eddy detection in MIZ using satellite altimetry is impeded by low resolution and the distortion of the signals by the sea-ice (Bashmachnikov et al., 2020). Eddy detection as spiral structures in Ocean Color and SST satellite images is limited by the visual procedure of their identification, the cloud cover and by uncertainties of how the surface signal maps to subsurface eddy structures (Morozov & Kozlov, 2023). The cloud cover is transparent for SAR signal, but the visual procedure of eddy identification, as well as various limitations in eddy recognition, impede massive remote detection of eddies in SAR data (Atadzhanova et al., 2017; Dokken & Wahl, 1996; Johannessen et al., 1996; Karimova, 2012). The most common mechanism of eddy manifestation in SAR is associated with the presence of slicks of surface films in the areas of water convergence (Espedal et al., 1998; Karimova, 2012; Kozlov et al., 2012; Munk et al., 2000; Zhurbas et al., 2019). This mechanism permits detecting

ocean eddies only under weak (but non-zero) and moderate winds (Karimova & Gade, 2016). In the MIZ, the sea-ice serves a tracer which makes eddy signatures visible in SAR images independent from the wind velocity (Petrenko & Kozlov, 2021; Zhurbas et al., 2019). However, even in the MIZ, eddy identification in SAR is biased toward detection of cyclones (Bashmachnikov et al., 2020; Kozlov et al., 2019). Therefore, despite a growing quality of satellite data, high-resolution ocean modeling remains an important instrument for study of eddy dynamics in the MIZ (Gupta & Thompson, 2022; Hattermann et al., 2016; Manucharyan & Thompson, 2017; Smith et al., 1991).

In this study we further explore a link between the variability of the sea-ice extent in the MIZ of the western Greenland Sea and eddy dynamics, using a high-resolution ocean model. We use a very high resolution configuration (1 km) of the ocean model FESOM (Finite Element Sea-ice Ocean Model), version 1.4 (Danilov et al., 2004; Wekerle, 2013, 2017, 2020). Validations of this model configuration showed a significant improvement against its older $4.5 \times 4.5$ km counterpart in reproducing the observed spatio-temporal distributions of the mean currents, RAW properties and eddy kinetic energy in the Fram Strait, as well as their seasonal variability (Wekerle et al., 2017). The eddy properties and generation mechanisms in FESOM were found to be in good agreement with a $0.8 \times 0.8$ km ROMS $\sigma$-model on a regular grid. Compared to ROMS results, FESOM was found to represent the sharper Polar front, in accordance with the observations at the Fram mooring section along 79°N (Wekerle et al., 2020). The serious underperformance of coarser resolution models in the Fram Strait additionally highlights the critical role of mesoscale and submesoscale processes in this area.

The manuscript structures as the following. Section 2 gives a brief outline of the FESOM1.4 configuration (2.1) and of the procedure used for estimating ice dynamics (2.2) and eddy detection (2.3). Section 3 starts with model validation for the study region (3.1–3.3), followed by analysis of the time variability of sea-ice advection (3.4), sea-ice formation/melt and background atmospheric and oceanographic conditions (3.5). Effect of eddies on the ice edge is discussed in Section 3.6. Section 4 presents the conclusions.

## 2. Data and Methods

The study region covers 75–78°N and 20°W–10°E, extending along the outer shelf of Greenland (Figure 1). The choice of the region was selected using the following considerations. First, it is characterized by the year-round ice cover along the EGC and high gradients of ice concentration in the MIZ that allow a robust detection of the ice margin. Second, the study region, being the area of contact of the RAW with Polar Water, is an area of high SST gradients. Finally, the Fram strait is recognized as the area of high eddy activity. The combination of these factors enhances the role of eddies in the sea-ice dynamics in the MIZ.

The spring-summer of 2007, a relatively warm year, were chosen for the analysis, covering the periods moderately negative atmospheric temperatures (April–May 2007), leading to the predominant sea-ice growth, and positive atmospheric temperatures (June–July 2007), leading to sea-ice ablation. The MIZ position during these months was relatively stable assuming a balance between dynamic and thermodynamic processes. Since mid-July the MIZ started a rapid retreat and losses its integrity, which dynamic period was excluded from the present analysis.

The microwave satellite AMSR-E data, used in this study for additional validation of the seasonal and interannual position of the sea-ice edge (Section 3), were downloaded from: https://data.seaice.uni-bremen.de/amsre/. The data set provides daily sea-ice concentration at $3 \times 3$ km spatial resolution (Spreen et al., 2008).

### 2.1. FESOM1.4 Ocean–Sea-Ice Model

Sea-ice concentration and eddy statistics were obtained from the global Finite Element Sea Ice-Ocean Model (FESOM1.4) developed at the Alfred Wegener Institute (Danilov et al., 2004; Timmermann et al., 2009). FESOM1.4 is an unstructured tetrahedral hydrostatic primitive-equation ocean and sea-ice model. The model mesh resolution (i.e., the size of triangles) ranges between 1 km in Fram Strait up 100 km close to the equator (Wekerle et al., 2017, 2020). In vertical the model is composed of 47 z-level with vertical resolution of 10 m in the upper 100-m layer and increasing with depth. Daily model outputs are used in this study. The model is forced by COREv.2 atmospheric reanalysis (Large & Yeager, 2008).

The sea-ice model is a dynamic-thermodynamic model with a prognostic snow layer, and uses an elastic-viscous-plastic sea-ice rheology (Hunke & Dukowicz, 2002). In FESOM1.4, sea-ice thermodynamics, that is melting and

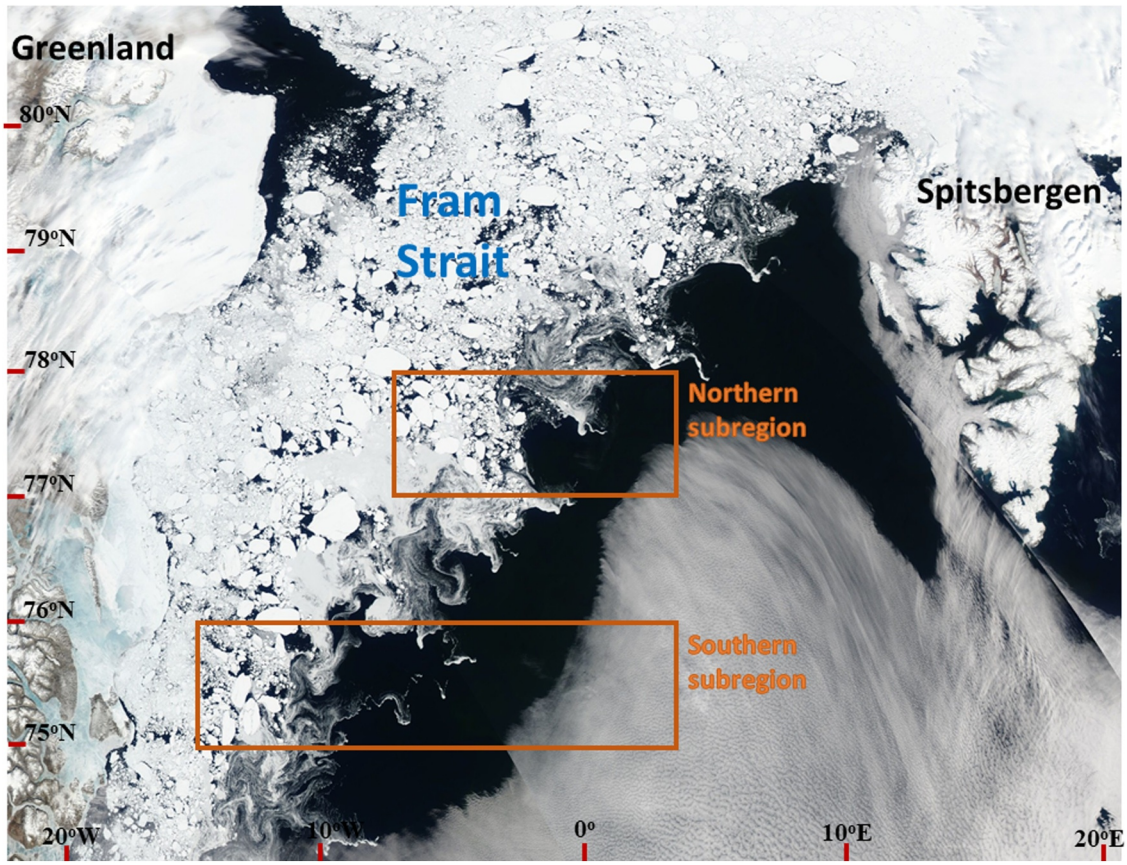


**Figure 1.** The study region in the northern Greenland Sea as seen in Suomi NPP True Color image acquired on 14.06.2019 with numerous eddying features in the marginal ice zone. The brown rectangles mark the study subregions.

freezing of sea ice, are based on energy balances for the ice-ocean and ice-atmosphere interfaces following the work by Parkinson and Washington (1979). The heat flux in the ice-covered grid cell between atmosphere and sea-ice consists of net shortwave and longwave radiation prescribed by the atmospheric forcing CORE2, turbulent fluxes of sensible and latent heat which are computed based on bulk formula according to Parkinson and Washington (1979), and a conductive heat flux. The heat flux between ocean and ice basically depends on the friction velocity and the temperature difference between the ocean surface and freezing point temperature. The ice growth rate is then calculated separately for ice-free and snow/ice-covered areas. Contributions from the ice-atmosphere interface and the ice-ocean interface are summed up. Following Hibler (1984), ice growth rate is computed for seven ice thickness classes instead of taking the effective thickness. A detailed description of the sea-ice thermodynamics can be found in Wekerle (2013).

The FESOM1.4 run, used in this study, was performed without any assimilation of in situ or satellite data. The model validation against remote sensing data showed that the seasonal cycles, as well as interannual variability, in the sea-ice extent and thickness are well captured by the model (Parkinson et al., 1999; Timmermann et al., 2009). The model used in this study has been extensively validated with ocean observations: hydrographic, velocity and EKE data from moorings deployed in Fram Strait, satellite derived eddy characteristics (Bashmachnikov et al., 2020; Wekerle et al., 2017, 2020).

### 2.2. The Sea-Ice Edge Variability

Depending on the goal of the study, various sea-ice concentrations were used to mark the ice-edge, ranging from 10% to 50%. Taking into account sharp gradients of the sea-ice concentration in the MIZ along the EGC, which drops from 50% to 10%–20% within a typical distance of 10–50 km, the choice of the critical ice concentration for outlining the ice edge can be rather delicate. For our purpose, the analysis is simplified when the sea-ice edge is

represented by a smooth uninterrupted line. Tests with FESOM sea-ice data showed that a 25% threshold is the optimum choice, being the minimum concentration that most of the time of the analysis keeps the ice edge directly linked to the area of the packed ice.

For further analysis two subregions were selected: northern (77–78°N) and southern (75–76°N) (Figure 1). As the western boundary of the region, different alternatives between 5° and 15°W were tested, for each of which the ice edge position remained east of the boundary over the study region during the whole study period. The eastern boundary was fixed at 3°E, so that no ice was crossing this boundary during the study period. The subregions were characterized by different water temperature gradients and different levels of eddy activity. Both characteristics were higher in the northern subregion, which is the focus of our analysis due to its high dynamism (see also Petrenko and Kozlov (2023)). The number of eddies in the southern region might be biased by a decrease of the FESOM1.4 resolution south of 75°N. However, a decrease in the number of eddies is conformed with SAR observations for 2007, as well as with 23-year mean altimetry observations (Bashmachnikov et al., 2020).

The daily section-integrated meridional sea-ice area transport ($Q_n$ and $Q_s$—across the northern and southern boundaries of the study subregion, respectively) and the zonal sea-ice area transport ($Q_w$—across the western boundary of the study subregion) were estimated using FESOM meridional ($V$, positive northwards) or zonal ($U$, positive eastwards) sea-ice velocities and the sea-ice concentrations (SIC):

$$Q_{n,s} = \Sigma(V \times \mathrm{SIC} \times G)$$

$$Q_w = \Sigma(U \times \mathrm{SIC} \times G). \quad (1)$$

Here $G$ is the distance between the neighboring mesh-points.

The convergence (positive is into the region) of the sea-ice area in each of the selected rectangular subregions was then estimated as:

$$Q = -(Q_n - Q_s) + Q_w. \quad (2)$$

The minus in front of the brackets suggest positive meridional convergence with the negative southward velocities across the northern section dominating the drift. We use sea-ice area as a more robust parameter, better validated with observations. These variations well reflect the modeled sea-ice volume fluxes, highly correlated with the sea-ice area fluxes across the corresponding boundaries of the subregions with the correlation coefficients of 0.97–0.98.

### 2.3. Eddy Detection in FESOM Data Sets

The eddy characteristics were derived daily using the sea-surface velocity of the FESOM1.4 model output. The automatic identification of eddy centers was performed with the kinematic algorithm by Nencioli et al. (2010). The algorithm identifies elliptic or circular rotating velocity patterns of a limited size. The spatial resolution of FESOM1.4 allows identification of eddies with the radii over 3–4 km. Eddy dynamic radii were derived as the mean distance from the eddy center of zero-crossing of the relative vorticity anomaly (Bashmachnikov et al., 2017). The radii of the maximum azimuthal velocity were then estimated by dividing the obtained values by $\sqrt{2}$, assuming Rayleigh azimuthal velocity profile (Bashmachnikov & Carton, 2012).

## 3. Results

### 3.1. The Interannual Variability of the Ice Edge Position Derived From FESOM and AMSR-E

To emphasize the important role of mesh resolution, we added a comparison between the eddy resolving FESOM1.4 configuration with 1 km spatial resolution, used in this study, and the previous eddy-permitting FESOM1.4 configuration with 4.5 km resolution (Figure 2). The Rossby radius of deformation in this region is 7–10 km. In the eddy-permitting configuration, the westward eddy-fluxes are not well resolved, leading to the less AW in the central Fram Strait. Thus, the RAW intrusion between 79° and 81°N, formed by mesoscale eddy dynamics, is detected only in the finer resolution model. As a result, the 4.5 km FESOM configuration shows a large bias of the simulated ice edge (Figure 2a), which is practically absent in the 1 km FESOM used in this study

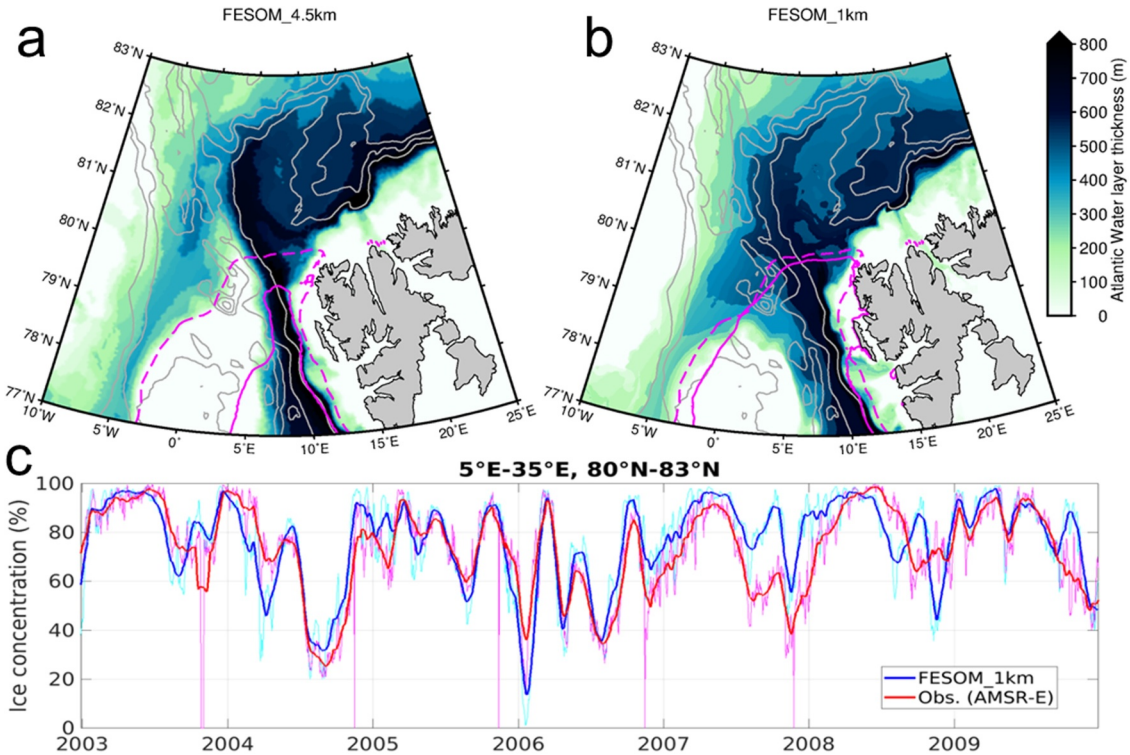


**Figure 2.** FESOM1.4 configuration at 4.5 km resolution (a) and at 1 km resolution (b) in the Fram Strait. Thickness (m) of the Atlantic Water layer is shown in color and the multiyear mean (January–March 2000–2009) position of the ice edge (here 15% concentration threshold is used) is marked with a solid pink line, while that derived from the AMSR-E satellite data is marked with a dashed pink line. (c) Time evolution of sea-ice concentration in the area north of Spitsbergen (5–25°E, 80–83°N): in 1-km FESOM daily means (cyan line) and 30-day sliding means (blue line) and in AMSR-E daily means (pink line) and 30-day sliding means (red line).

(Figure 2b). Thus, reproducing the mesoscale variability is crucial for correctly reproducing the recirculation of the warm Atlantic Water in the Fram Strait (von Appen et al., 2015; Kolas & Fer, 2018). The comparison above suggests a potentially strong influence of mesoscale eddy transport on the position of the sea-ice edge in the study region.

The 1 km FESOM1.4 configuration also correctly reproduces the interannual variability of sea-ice concentration north and northwest of Spitsbergen (Figure 2c). This is the area of a direct sea-ice supply into the study region along the shelfbreak branch of the EGC. The decline in the Arctic sea-ice extent has been noted since the late 1970s over most of the marginal seas of the Eurasian Arctic (Parkinson et al., 1999; Shalina, 2021), as well as in the Greenland Sea south of 77°N. North of these latitudes a certain increase in the Greenland Sea sea-ice concentration is observed due to an intensification of sea-ice flux across the Fram Strait (Selyuzhenok et al., 2020). During the 7 years, presented in Figure 2c, no trend in the sea-ice concentration in the northern Fram Strait is observed in both, FESOM and satellite data. This suggests that the analysis of the sea-ice conditions of 2007 below is also representative for other years of the modern period.

### 3.2. Seasonal Variability of the Ice Edge Position Derived From FESOM and AMSR-E Data During 2007

The sea-ice extent in the study subregions remained rather stable from January to June/July in both, FESOM1.4 simulations and AMSR-E satellite observations, followed by a rapid retreat toward Greenland in August, and a swift recovery already in September/October 2007 (Figures 3a and 3b). Besides of a certain bias in the position of the ice edge (on average, 1–2° longitude (25–50 km) east from the observed position, Figures 3a–3b) and a 1.5 times overestimate of the sea-ice concentration along the ice edge (Figures 3c and 3d), FESOM well represents details of the observed seasonal cycle of the sea-ice edge dynamics, as well as the level day-to-day dispersion of the ice properties in the northern (Figures 3a and 3c) and southern Figures 3b and 3d) study subregions. These minor deviations between the modeled and observed large-scale seasonal and spatial variability of the ice edge indicate a high degree of reliability in the model results for the Fram Strait.

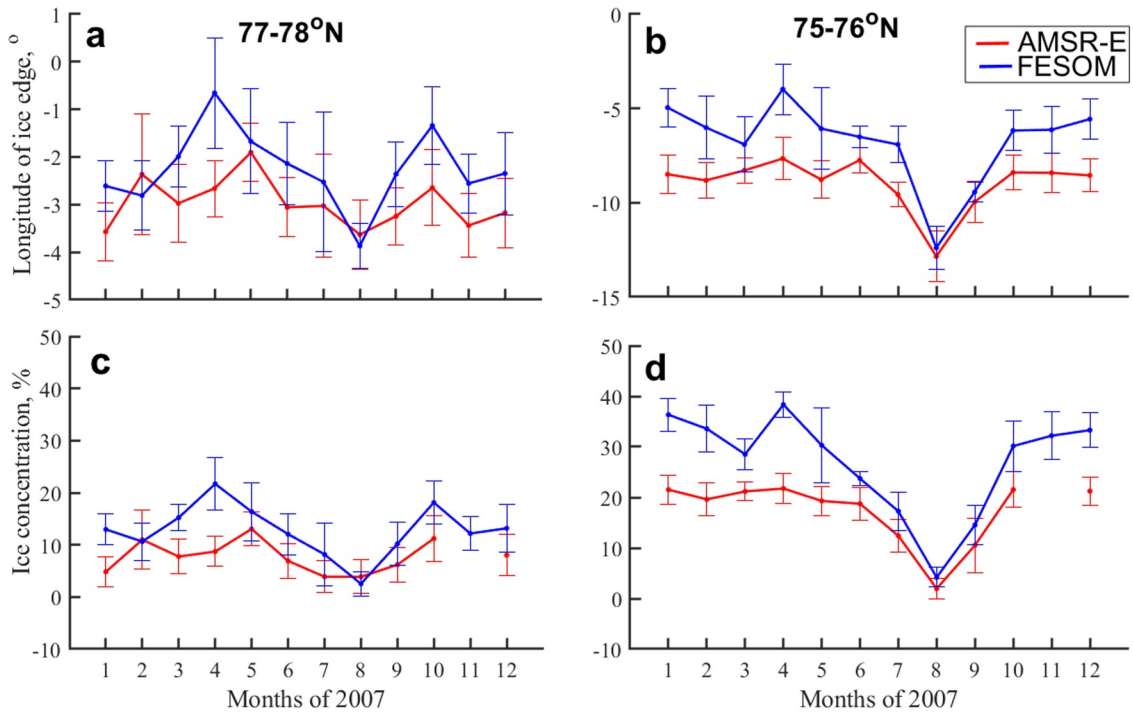


**Figure 3.** Seasonal variability of the monthly and regional mean longitude position (degrees) of the sea-ice edge during 2007 in FESOM1.4 (blue lines) and AMSR-E (red lines) in the northern Greenland Sea (north to south): (a) 77–78°N, (b) 75–76°N, and the sea-ice concentration (c) 77–78°N, 15°W–5°E, (d) 75–76°N 15°W–5°E. The error bar marks the standard deviation of the parameters within the month.

### 3.3. Eddy Properties in FESOM

Given the baroclinic Rossby radius of deformation on the order of several kilometres in the Fram Strat, the 1-km mesh resolution in FESOM1.4 allows reproducing mesoscale features, as well as a range of submesoscale eddies, which results can be compared to SAR data. The SAR eddies were visually identified with their spiral patterns. Following Kozlov et al. (2019), eddy radii in SAR images were detected as the outmost spiraling isolines, interpreted as the streamlines. Eddy radii defined this way correspond to eddy dynamic radii, defined in FESOM data as the mean position of the contour, where relative vorticity of an eddy core changes its sign. Both SAR and FESOM eddy data sets demonstrate very similar spatial patterns of the time mean eddy concentrations and eddy radii. A detailed comparison with SAR data for 2007 was done in Bashmachnikov et al. (2020). The number of eddies is comparable to that detected in the Fram Strait and along the WSC. Eddies are relatively less frequent within the EGC but reach a local maximum in occurrence immediately east of the jet (see also Petrenko & Kozlov, 2023). Eddy radii increase northward toward the Fram Strait in both, the FESOM1.4 simulations and SAR data sets. However, FESOM data shows larger radii in the EGC, while SAR data suggests a local minimum of eddy radii in the EGC and a local maximum east of the current. The difference may be a result of larger eddies being more difficult to be detected in SAR due to an intermittent sea-ice cover over the EGC. Histograms of eddy radii in SAR peaks at 1–3 km scales, while those on FESOM peaks at 10–12 km (Bashmachnikov et al., 2020). In addition, FESOM simulations indicate that approximately 60% of all detected eddies are cyclonic, whereas SAR observations suggest a higher proportion of cyclones comprising about 80% of the eddy population. These differences may be a consequence of a bias in eddy detection in SAR data toward smaller eddies and toward cyclones, even when the sea-ice is used as a tracer (Bashmachnikov et al., 2020; Kozlov et al., 2019; Manucharyan & Thompson, 2017; Zhurbas et al., 2019).

Figure 4 shows an example of eddies in the MIZ along the EGC between 20 and 23 of July 2007 in SAR (Figures 4a and 4b) and FESOM data (Figures 4c and 4d), where the red boxes mark the same geographic area. First, the good agreement between SAR and FESOM1.4 data in the mean position of the ice edge within the red squares, along with a consistent eastward decrease in the sea-ice concentration in both data sets from around 70%–80% to less than 50% within the MIZ. In both data sets, eddies are forming filaments of drifting ice of approximately the same scale of

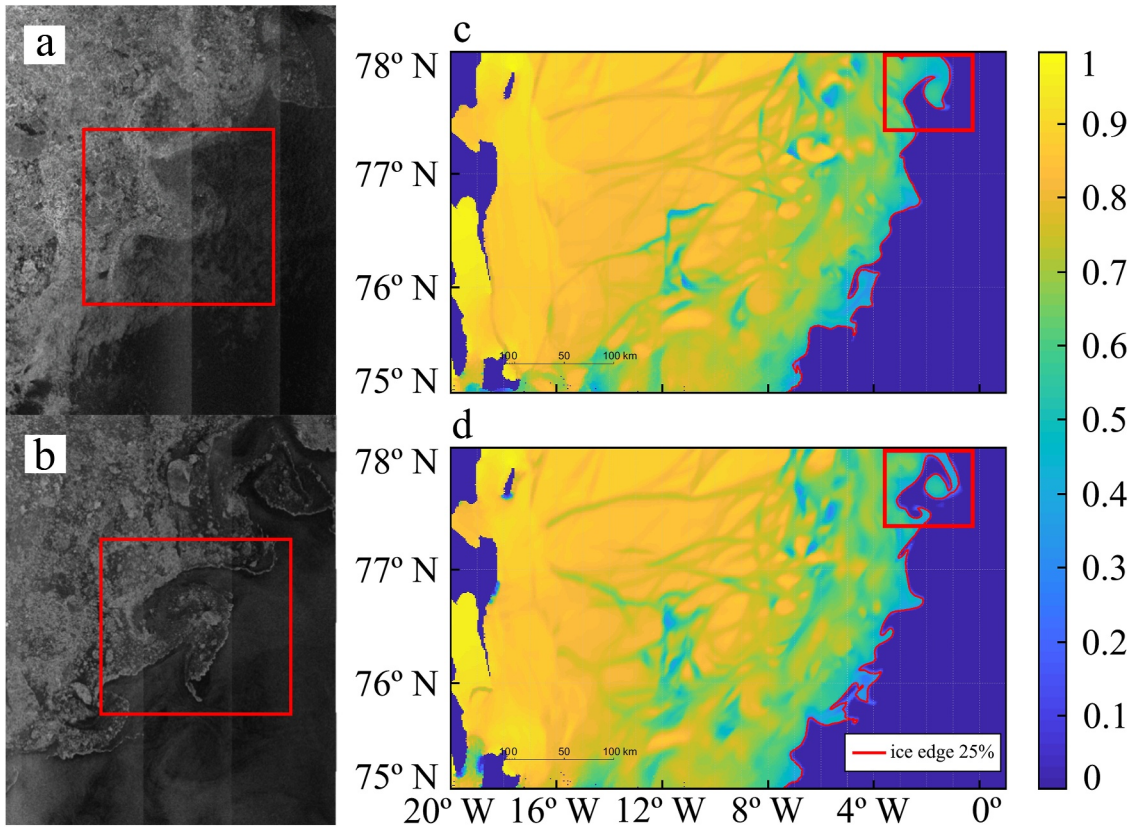


**Figure 4.** Eddies in the marginal ice zone area at 77–78°N in synthetic aperture radar (SAR) images at (a) 20th and (b) 23rd of July 2007. Sea-ice concentration in FESOM data at the same dates (c) 20 July 2007 and (d) 23 July 2007. Red squares in SAR and FESOM data mark the same geographical area.

around 50 km that extend east from the ice edge. The ice filaments initially formed around a single cyclonic eddy and subsequently evolve into mushroom-like dipole structures, which disperse and promote the melting of the trapped sea ice. In SAR data (Figures 4a and 4b), the dipole is formed in the MIZ and then propagates eastwards, away from the ice edge. In this configuration, the cyclonic eddy pulls the ice eastwards along its southern margin forming a leg of the mushroom-like structure. In FESOM data (Figures 4c and 4d) the anticyclone is formed with the MIZ. Then, during its interaction with the EGC, a pare cyclone is formed to the south (see Smith et al., 1991). Together they form a dipole with the leg extending from the open water toward the ice edge (Figure 4d). This example shows that the model is able to reproduce well the highly nonlinear processes of eddy generation and eddy-current interactions, as well as reproduces the size and dynamics of eddy trapped sea-ice filaments, which is the main focus of this study.

### 3.4. Ice Advection Across the Boundaries of the Study Regions

In FESOM data, the number of eddies in the MIZ strongly decreases from north to south. In this study we performed a detailed analysis for the northern subregion (77–78°N and 6°W–3°E). The southern subregion (75–76°N and 6°W–3°E) has a much weaker eddy activity and is given only for comparison.

The spatial and temporal variability of the sea-ice extent in the Greenland Sea, as well as of its subregions, is the result of local sea-ice formation or melt and the convergence of the drifting ice. To estimate the role of eddies in the sea-ice melt, we preliminary eliminate the effect of the sea-ice transport across the boundaries of the study region (Section 2.2). The regional spatial and temporal variability of the sea-ice drift is significant, forced by winds and ocean currents.

From the beginning of April to the end of July 2007 the ice edge was relatively stable (Figure 3), while the air temperature was close to zero (see Section 3.5). We intentionally avoid the periods of intensive winter ice

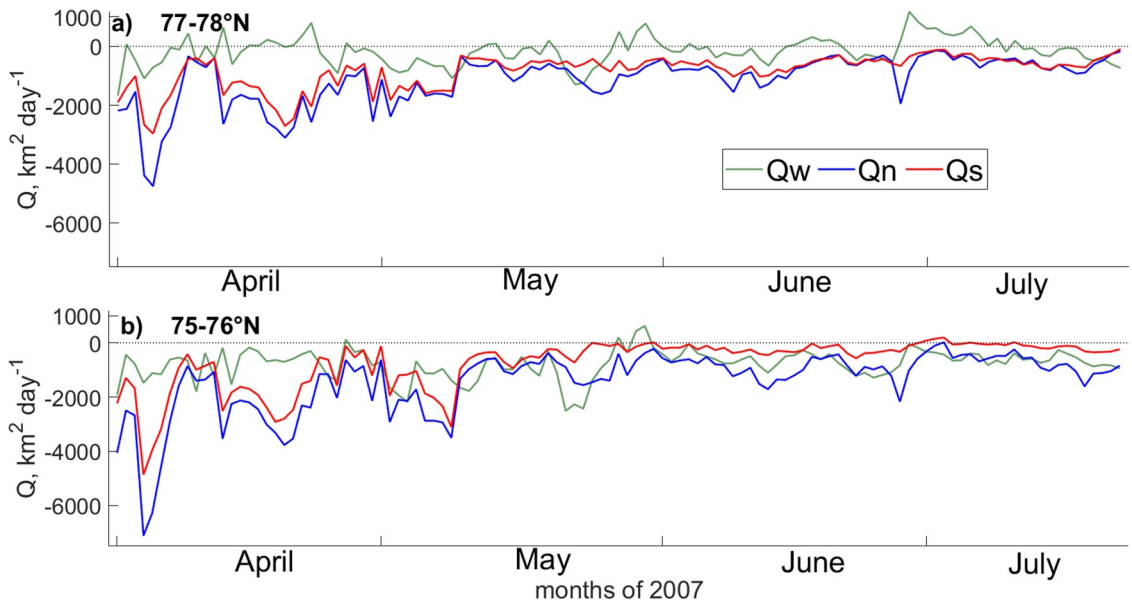


**Figure 5.** The fluxes of the sea-ice area (km$^2$ day$^{-1}$) across the northern ($\boldsymbol{Q_n}$, blue lines), southern ($\boldsymbol{Q_s}$, red lines) and western ($\boldsymbol{Q_w}$, green lines) boundaries of: (a) the northern marginal ice zone (MIZ) subregion at 77–78°N; (b) the southern MIZ subregion at 75–76°N. The negative sign means southwards (for $\boldsymbol{Q_n}$ or $\boldsymbol{Q_s}$) or westwards (for $\boldsymbol{Q_w}$) transport.

formation or rapid ice melt in late summer, as we expect that during the transitional period the role of ocean eddies in the dynamics of the sea-ice edge is the most evident.

The migration of the eastern boundary and the resulting change of the sea-ice area in the study region is expressed as a sum of sea-ice transport across the boundaries of the study region ($Q$) and the local new ice formation or ice melt ($Q_{\text{th}}$):

$$dS = Q + Q_{th}. \tag{3}$$

Changes in the sea-ice area $dS$ can be estimated directly from FESOM as the difference in ice areas at day $i + 1$ and day $i$. To be consistent with $dS$ estimates, we average the components of $Q$ between days $i$ and $i + 1$. $Q_{\text{th}}$ is found as the residual term, while we investigate the role of eddies in its variability. The correlation between the changes of the sea-ice area above and the sea-ice volume in the study region is 0.92.

At the beginning of the study period the fluxes across the northern ($Q_n$) and southern ($Q_s$) boundaries clearly dominate in $Q$. In the northern subregion, these fluxes become comparable with the ice-area flux across the western boundary ($Q_w$) since the end of April (Figures 5a and 5b). In their absolute values, $Q_n$ exceeds $Q_s$ most of the time; this difference typically is below 10% of $Q_n$. This suggests that most of the sea-ice simply crosses the subregions on its way south from the Fram Strait, but some fraction of it melts within the study subregions. A significant fraction of the day-to-day variability of the ice area is also linked to $Q_w$, which accounts for the sea-ice migration across the EGC. Since the western boundary of the subregions is chosen in such a way, that it is always within the sea-ice at high concentration (over 50%), $Q_w$ should be mostly linked to the changes in the direction of meridional winds. Most of the time the sea-ice at the western boundary is pushed toward the Greenland shelf ($Q_w < 0$), which is a sign of the dominating northerly winds, typical for the study region. In the northern subregion, where the EGC is directed south, we may expect that the periods with $Q_w > 0$ result from episodic bursts of the southerly winds pushing the sea-ice eastwards across the western boundary (Figure 5a). In the southern subregion, the south-southwestwards direction of the EGC suppresses the eastwards ice migration (Figure 5b). Northerly winds bring low-temperature air and, besides amassing the ice closer to the coast, increase local new ice production. Southerly winds not only disperse the sea-ice into the area of a bigger influence of the warm RAW, but also bring warmer air which intensifies the ice melt.

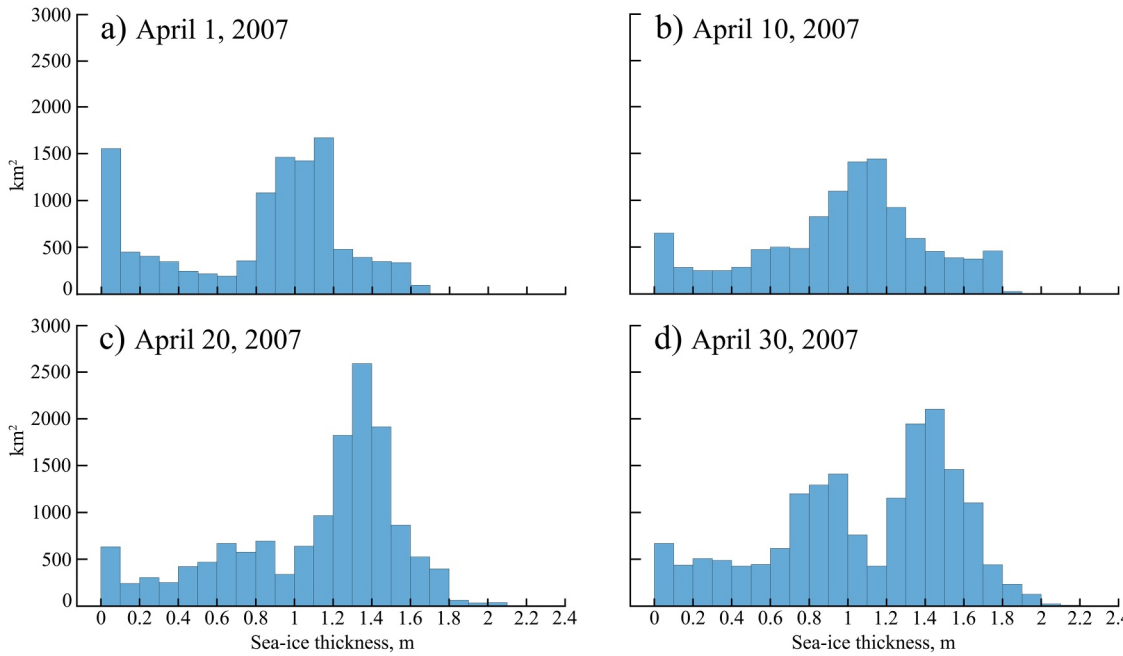


**Figure 6.** Histograms of the areas ($km^2$) of the sea-ice with different thickness (m) in FESOM in the northern subregion in April 2007: (a) April, 1, (b) April, 10, (c) April, 20, (d) April, 30.

The daily sea-ice convergence ($Q$) accounts for, on average, less than 10% of the total sea-ice area in each of the subregions. Nevertheless, the day-to-day variability of $dS$ and $Q$ are highly correlated (the correlation coefficient exceeds 0.8), which suggests that the balance between ice area advection across the region boundaries forms the major input in the dynamics of the sea-ice area in the study region.

The thermodynamic sea-ice area change ($Q_{th}$) will be of our main interest in this study. $Q_{th}$ is negative most of the time, which suggests an overall ice melt in the study region compensates the convergence of the advected ice and maintains the MIZ edge in approximately the same position during the spring-summer study period (Figure 3).

To evaluate the consequences of different choices of the western boundary, the variability of $Q$ for different positions of the western boundary was estimated. With some small differences in the absolute values, the time evolution of $Q$ was practically independent of this choice. The mean error linked to the alternative positions of the western boundary in the northern subregion was less than 1% of $dS$ and less than 5% of $Q_{th}$. Further results for the northern subregion are presented for the western boundary at 6°W, which is the westernmost position still not crossed by the ice edge during the whole study period.

### 3.5. Ice Formation and Melt During Spring-Summer 2007

Histograms show significant variations in ice thickness during April 2007 (Figure 6). At the beginning of April the ice thickness had a clear bimodal distribution (Figure 6a), caused by a combination of a locally formed new nilas (less than 10 cm thick) and the 1-year sea-ice (about 1 m thick), transported from the Arctic. By the 10th of April the fraction of nilas decreased sharply and continued decreasing until the end of April, while another peak at 1.5 m sea-ice emerged (Figures 6b–6d).

To assess the effects of air and water temperature on the variability of sea-ice concentration, we used the sea surface water temperature from FESOM and near-surface air temperature from ERA-Interim (https://www.ecmwf.int). At the beginning of the study period (in April 2007), air temperature was always negative changing between −15 and −5°C (Figure 7a). It remained negative (−5 to 0°C) until May. In June and July 2007, air temperature rose slightly above zero over most of the northern subregion, making 1–3°C in the monthly spatial means. Thus, the atmosphere added to the sea-ice formation over the first half of the study period and to the sea-ice melt over its second half. The SST, all over the study period, ranges from the freezing temperature (−1.8°C) in the drifting ice to 0–5°C in the eastern part of the region (Figure 7b). A freezing SST is limited to the western part

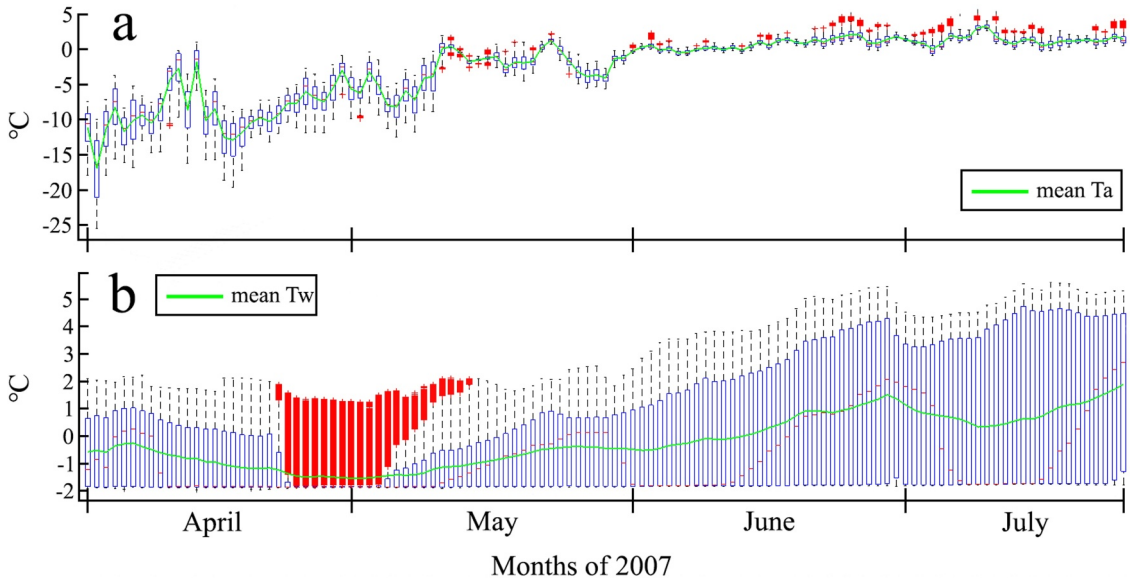


**Figure 7.** Air temperature from ERA-Interim (a) and the sea-surface water temperature from FESOM1.4 (b), from 1st of April to 24th of July 2007 in the northern subregion (77–78°N). Green lines show the mean, red hatches are the median, blue rectangles are interquartile distances and dashed lines mark the full range of temperatures within the northern subregion of each particular day of the study period. With the bigger range, covered by the blue squares and dashed lines, the temperature gradients in the marginal ice zone area increase.

of the region, covered with the sea-ice during the whole study period. The interquartile range is 2–3°C in April–May more than double in July, which suggests a corresponding increase of the water temperature gradients across the northern subregion. The rise of the mean water temperature from −1 to 1°C over the study period, while the MIZ does not change its position, suggests the overall warming of the open water area (Figure 7b).

In April–May 2007, the sea-ice can form everywhere in the region, where the sea-surface water is cold enough, as the air temperature is below the seawater freezing point of −1.8°C. During this period the sea-ice dynamics should be closely coupled with ocean dynamics, including the cross-frontal mixing by eddies. During June and July, when the air temperature is just above 0°C, possible areas of formation of the new sea-ice in the model should be restricted to the areas between the ice floes, where water is at its freezing point. We may then expect a more extensive nilas formation when the sea-ice floes start being advected eastwards across the EGC. The southerly winds dominate the area, for example, at the eastern side of atmospheric cyclones passing across the western Greenland Sea. However, the rise of the air temperature and sharper water temperature gradients surrounding the ice floes would also add to the melting of sea-ice as soon as it becomes more dispersed. Therefore, at this second period, wind might strongly affect the freezing/melting rate in the selected regions, and $Q_{th}$ may become partly decoupled from the ocean dynamics, including the mixing rate by mesoscale eddies.

### 3.6. Effect of Eddy Transport on the Ice Edge

The effect of mesoscale eddies on the ice edge consists in advecting warmer water to the MIZ and beneath the sea ice, as well as in sweeping sea-ice into the warmer water area. In this study we do not consider vertical heat fluxes in anticyclones under the compacted sea-ice (Gupta et al., 2020), which are low in the mesoscale eddies in quasi-geostrophic balance dominating in the model results. In the MIZ, eddies also contribute to a nonuniform sea-ice motion that compacts ice in the convergence zones and forms more open water in the divergence zones. This can enhance the sea-ice melting or freezing potential, depending on the air temperature. In the next sections we investigate a link between eddy activity and the position of the sea-ice edge along the EGC.

#### 3.6.1. Case Studies of Eddies Shaping the Sea-Ice Edge

A preliminary visual analysis of SAR and FESOM images suggests that MIZ eddies have a very strong effect on ice dispersion by trapping ice at the sea-ice edge and forcing it into a circular movement around their centers (see example in Figure 4). Figure 8 presents a typical example of eddy activity over all 3 subregions (75–76°N,

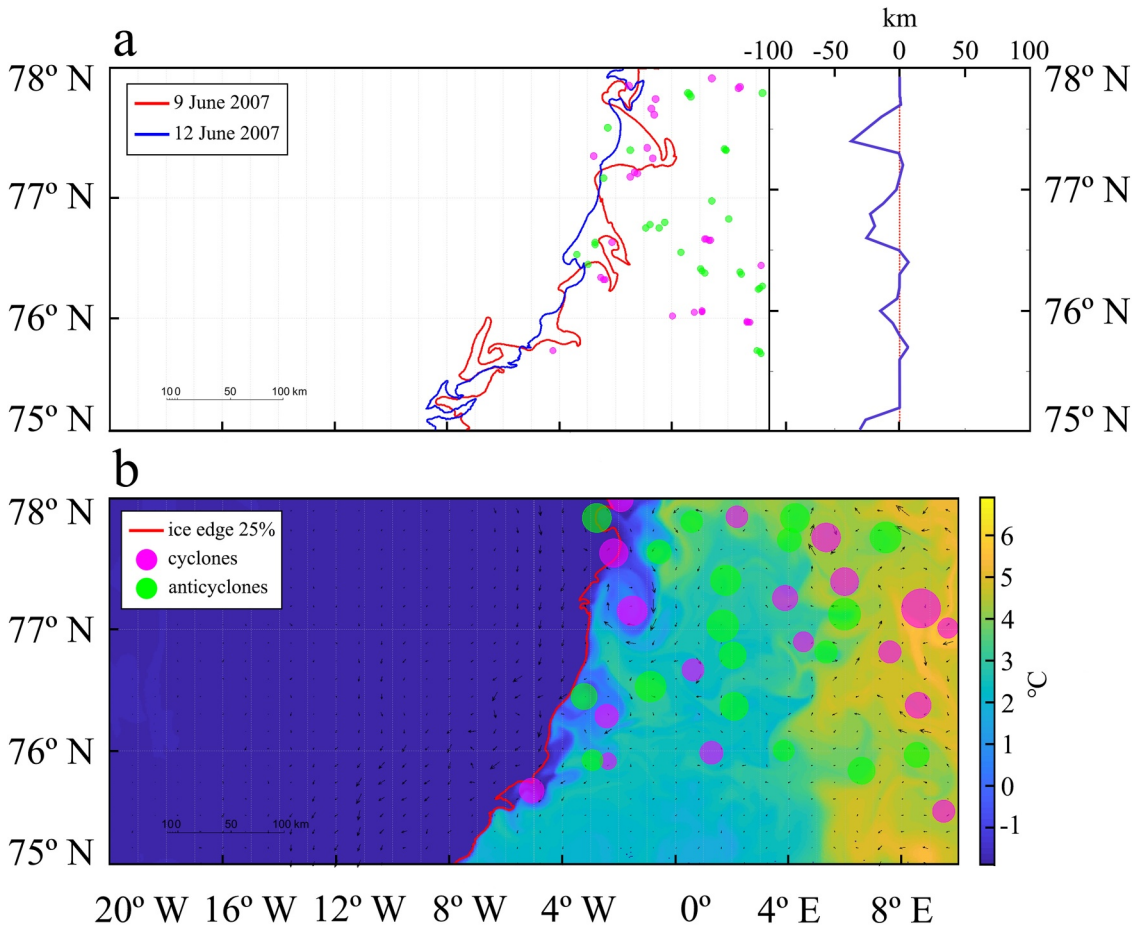


**Figure 8.** (a) Two consequent positions of sea-ice edge in FESOM at year-day 160 of 2007 (9 of June, red line) and day 163 (12 of June, blue line) and positions of all centers of mesoscale eddies between day 160 and 163 (magenta - anticyclones, green—cyclones). Note that some of the close positions of eddy centers means the same moving eddy. The right panel shows the migration of the ice edge (in km) at the particular latitude during the 3-day period (days 160–163). (b) Water temperature (°C, color), sea-ice edge (25% of ice concentration—red line, the line does not to account for ice floes separated from the main sea-ice packed sea-ice) and positions of cyclonic (green filled circles) and anticyclonic (magenta filled circles) eddies in FESOM data on the 17 of June 2007 (day 168). The size of the circle is proportional to eddy dynamic radii. Black vectors are FESOM currents.

76–77°N, 77–78°N). Two regions of the strongest retreat of the ice edge, between 76.6° and 77°N and around 77.5°N, are also the areas with numerous eddies reaching the MIZ. The retreat of the ice edge within 3 days, after being trapped by eddies, suggests its rapid sea-ice dispersion and melt within the eddies (Figure 8a). Figure 8b shows how eddies, as the one centered at 77.2°N and 2°W, form the cross-MIZ exchange by the rotating cold water (with ice floes) and advecting water with positive temperature (in the north of the study region the water temperature can reach 3–5°C) around their peripheries toward the MIZ. The water temperature of the cold filament in this anticyclone turns positive not even making a full turnover around the eddy center, which suggests a complete sea-ice melt in the filament within 1–2 days. Eddies separated by more than three dynamic radii do not affect the ice edge (see, e.g., the cyclone at 76.5°N, 1°W). Therefore, in further analysis, we consider only the eddies separated from the ice edge by no more than three mean eddy radii (see also Smith et al., 1991), which is around 100 km for eddies in FESOM data set.

An interaction with the ice edge of an anticyclone, generated within the ice-covered area just west of the ice edge, is demonstrated in four consequent maps of Figure 9, separated by the 3-day intervals. On the first map an anticyclone resides under the sea-ice in the EGC at 77.8°N, 0.2°E (Figure 9a). Then it moves southeast and distorts the ice edge, forming an ice blob extended eastwards from the ice edge (Figure 9b). This sharpens the temperature gradients and increases the area of the ice—warm water contact. Some of the warm water, trapped by the anticyclone, is pushed toward the ice edge along its southern limb. At this stage, the coupled cyclone begins to form along the southern boundary of the trapped warm water jet (Figures 9b–9d). Within the anticyclone, warm water

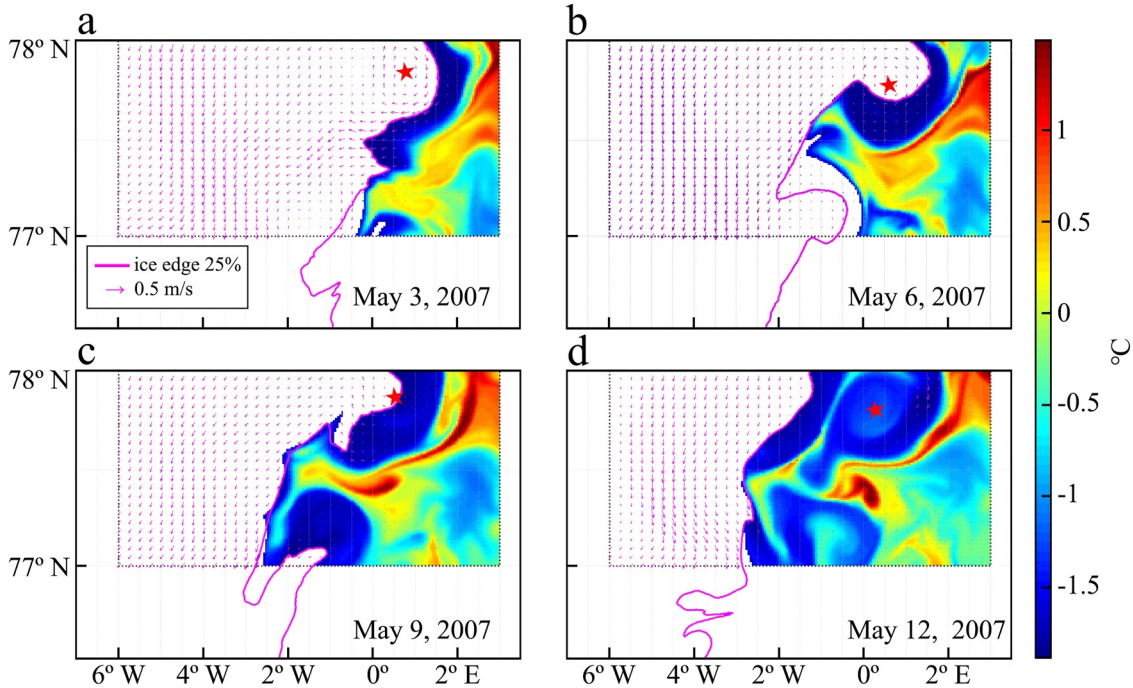


**Figure 9.** FESOM daily sea-surface temperature at (a) May 3 (day 123), (b) May 6 (day 126), (c) May 9 (day 129) and (d) May 12 (day 132) of 2007. The magenta vectors are the FESOM derived sea-ice drift (m $s^{-1}$) for the same dates, magenta line marks the sea-ice edge at 25% ice concentration. The center of the anticyclonic eddy, referred to in the text, is marked with a brown star.

intrudes between the eddy and the newly formed ice edge (Figures 9c and 9d), leading to complete sea-ice melts within the anticyclone and its vicinity during 9 days (Figures 9a and 9d). The ice edge retreats by 3° longitude, which is over 70 km (Figures 9a and 9d). The observed evolution took place in the first half of May, when the air temperature over the study region was below the freezing point (Figure 7a). This suggests that the ice melt was totally due to the effect of eddy heat advection. The sea-surface water temperature within the anticyclone was constantly rising from the freezing point on the 3rd of May (Figure 9a) to −0.5°C on the 12th of May (Figure 9d), and further reaches positive values (not shown). The consecutive figures show the advection of warm water plays a leading role in the evolution of the ice edge.

The cyclonic eddy 80 km south of the described anticyclone, within the dipole, additionally pushes some water of the warm jet southwards along the ice edge (Figures 9c and 9d). At the latitude of the cyclone the sea-ice locally retreats by 2° longitude. The overall area of the sea-ice melt by the anticyclone and the paired cyclone during 9 days is around 6,500 $km^2$, which forms over 700 $km^2$ per day. This exceeds the standard deviation of the convergence of the sea-ice transport within the northern subregion, which forms over the study period 440 $km^2$ per day, while its mean value is four times lower. The mean sea-ice thickness in this region of the MIZ was 90 cm, and the eddy induced ice volume melt is $V = 0.6$ $km^3$ per day. The standard deviation of the convergence of sea-ice volume transport over the study period is 1 $km^3$ per day. The estimates above show that eddies are able to transport enough heat toward MIZ to effectively compensate the sea-ice area/volume convergence in the northern Greenland Sea and maintain the MIZ stable.

### 3.6.2. Integral Effect of Eddies on the Ice Edge

Case studies of the previous sections suggest that heat transport and sea-ice advection by eddies regulate the position of the sea-ice edge along the EGC. The integral effect of eddies in the MIZ is estimated using the metrics of the total number of the detected mesoscale and submesoscale eddies ($N$) in FESOM data. The time series of integral eddy kinetic energy summed over all eddies closely follow the number of eddies. Therefore, as an additional parameter we estimate integral eddy kinetic energy for an average MIZ eddy: $\mathrm{IEKE}(i) = \frac{1}{N_i}\sum_1^{N_i}\left[\iint \frac{u_i'^2+v_i'^2}{2} dx\, dy\right]$,

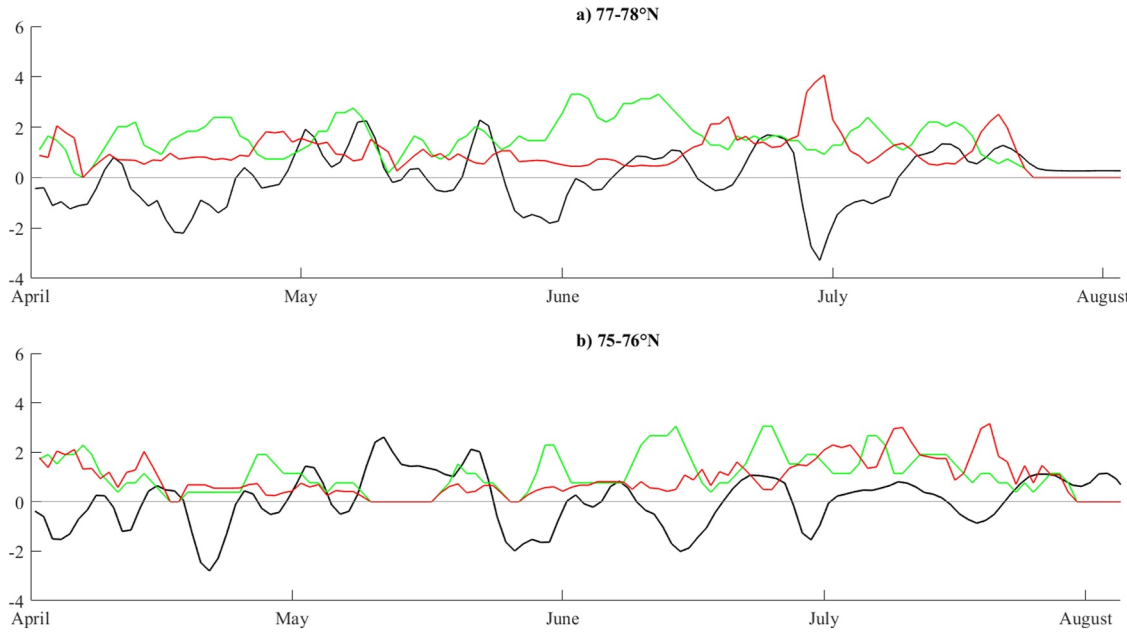


**Figure 10.** The sea-ice formation/melt (black line) from April–July 2007 in (a) the northern subregion at 77–78°N and (b) the southern subregion at 75–76°N. Green line is the number of eddies and red line is the mean integral kinetic energy of an eddy in MIZ (IEKE), defined with the 50-km distance from the ice margin. The normalized values are obtained by subtracting mean from the raw data and dividing the result by the standard deviation; the lowest values of the number of eddies and IEKE (no eddies in the MIZ) was set to zero.

where $u_i'$ ($v_i'$) represent the zonal (meridional) sea-surface current velocities integrated over the areas of each of $N_i$ detected eddies within the MIZ area (Figure 10) during day $i$.

In the study region, air temperature persisted below the seawater freezing temperature until mid-May (Figure 7a). In April the ice margin the northern subregion reached its most eastward position during 2007 of 1°W and then was retreating westwards until August (Figure 3a). $Q_{th}$ reached its highest value in the first half of May and further decreased in June and July (Figure 10a), coinciding with, when the air temperature grew above zero and water temperature gradients in the MIZ increased (Figures 7a and 7b). However, no clear tendency for $Q_{th}$ to decrease during spring-summer 2007 was observed, suggesting that the ice area retreat is mostly linked to a decrease in the sea-ice convergence in the study region (Figure 5). When taking 2-week sliding mean, $Q_{th}$ was oscillating around zero. These low-pass filtered intra-month tendencies of $Q_{th}$ are not linked to eddy dynamics, having practically zero correlations with eddy characteristics (Figure 10). The 2-week sliding mean filter was used. Correlation of the high-pass filtered intra-month variations of $Q_{th}$ with *IEKE* exceeds −0.5 with the critical correlation of 0.2 for the period April–July. This suggests a decrease on several day/weekly time scales in the ice area due to eddy induced ice melt when energetic eddies are detected in the MIZ.

FESOM1.4 results show that the number of eddies was always higher east of the EGC (Figure 8). In August 2007, as the MIZ retreats to the mid-shelf of Greenland, the number of eddies in the ice-free area west of the EGC decreases and for long time periods no eddies are detected (Figure 10), while east of the EGC the number of eddies remain at a higher level. Thus, we observe an approximate dynamic balance. When the MIZ migrates east, crossing the outer part of the EGC, the number of eddies in the MIZ increases, increasing the horizontal mixing and sea-ice melt, thus, stabilizing the MIZ. When the MIZ migrates westwards, the number of eddies decreases and convergence of the sea-ice advection stabilizes the MIZ. Therefore, we suggest that MIZ eddies limit the eastward migration of the MIZ rather than forcing its retreat. In the southern subregion, eddies are much less numerous, but similar tendencies are observed (Figure 10b).

## 4. Discussion and Conclusions

In this study we have explored the effect of eddies on the MIZ and the ice edge position in the north-western Greenland Sea using a FESOM1.4 ocean model configuration with high mesh resolution in the area (1 km).

Our region of interest is the EGC area of the northern Greenland Sea, where active interaction between the ice-covered Polar Waters with the Recirculating Atlantic Waters is observed. The computations were performed for 2007, when the atmospheric circulation forced a faster Transpolar drift in the central Arctic Ocean followed by an enhanced sea-ice discharge through the Fram Strait (Kwok et al., 2009). However, an increased rate of the sea-ice melt (Selyuzhenok et al., 2020) leads to a relatively stable position of the ice edge in the study region, registered in both FESOM results and AMSR-E satellite data. During 2007, the ice edge experienced a single deep retreat in August and returned back already in September. During spring 2007, the MIZ oscillated around its mean position with a very gradual retreat forced by variations in convergence of the sea-ice advection with the EGC from the Arctic, wind forcing and local sea-ice thermodynamics. During the study period, the sea-ice flux across the northern boundary exceeded that across the southern boundary, suggesting the sea-ice convergence in the study region with episodic eastwards bursts of the sea-ice drift as a result of wind forcing. These are followed by a more intensive ice melt, as it propagated over the warmer water in the west, as well as due to an intensification of the eddy activity (see also Gupta & Thompson, 2022). The relative stability of the MIZ suggests that the overall divergence/convergence of the sea-ice transport is largely compensated by the sea-ice formation/melt. Since the atmospheric temperatures were negative or close to zero from April–June 2007, ocean should play a significant role in the sea-ice melt during this period.

Observations and model results suggest that the effect of eddies on sea-ice edge may be significant (Johannessen, Johannessen, Svendsen, Shuchman, Campbell, et al., 1987; Manucharyan & Thompson, 2017, 2022). Several case studies presented here revealed that horizontal mixing by mesoscale eddies across the large-scale water temperature gradients exert a strong effect on the MIZ position. This is true for eddies formed under the ice within the MIZ, as well as for eddies that approach the MIZ from the open water. For example, the local ice edge retreat near an anticyclonic eddy amounts to about 3° longitude and at the nearby cyclonic eddy it retreated by about 2° longitude (Figure 9). Keeping in mind that 1° longitude in the northern Greenland Sea is around 25 km, the results suggest a local sea-ice retreat of 5–10 km day$^{-1}$, several times faster than previously estimated (Johannessen, Johannessen, Svendsen, Shuchman, Campbell, et al., 1987; Kozlov & Atadzhanova, 2022). However, in spite of a strong local effect of eddies on the position of the ice edge (Figure 9), no clear statistical link between the number of eddies (or the *IEKE*) and the position of the ice edge was detected on the time scales longer than 1 week. In the study region eddies exhibit a short-term effect on the position of the ice edge, quickly restored by the convergence of the sea-ice advection as the eddies decay.

Nevertheless, the stability of the ice edge in spring shows that eddies are able to converge enough heat in the MIZ to maintain it stable. Our results showed that as the MIZ progresses eastward toward the warmer area more densely populated with eddies, the ice melts at a higher rate, limiting this progress (see also Gupta & Thompson, 2022). With the westward retreat of the MIZ, the number of eddies decreases and the retreat is hampered by the sea-ice convergence. Thus, with the August retreat of the MIZ over the Greenland shelf, a strong reduction of the eddy activity west of the EGC is followed by a relatively fast return of the MIZ already in September. These results suggest that the main role of eddy-induced mixing consists in limiting the MIZ extent and impeding spreading of the sea-ice in the central areas of the Greenland Basin. The central preconditioning mechanism for such ice melt is a convergence of the warm RAW from the West Spitsbergen Current with the Polar Water of the East Greenland Current, while eddies intensify the cross-frontal heat exchange. Intensification of a front leads to its higher instability and an increase in the number of eddies in the MIZ.

The heat flux toward the ice edge required to melt the volume $V$ can be estimated as: $Q = L \rho_i V$, where $L = 3.4$ $10^5$ J kg$^{-1}$ is the specific heat of ice fusion and $\rho_I = 920$ kg m$^{-3}$ is the sea-ice density. In the example above the melted volume of 0.6 km$^3$ per day requires around 1 TW of heat to be transported toward the ice edge by each of the eddies (the anticyclone and the cyclone). The eddy transport plays a significant role in translating the RAW toward the EGC (von Appen et al., 2016; Hattermann et al., 2016). The mean zonal eddy heat flux across the same section of 1° latitude from the West Spitsbergen Current, as well as from the Norwegian Atlantic Front Current, is estimated as 1–3 TW, derived using satellite altimetry data (Bashmachnikov et al., 2023). This means that eddy transport of the RAW from the WSC in the Fram Strait forms a heat flux of sufficient intensity to stabilize the sea-ice convergence in the northern Greenland Sea. Note that, due to a small amount of combined altimetry and in situ data in the Fram Strait, the estimates of eddy flux from the WSC in Bashmachnikov et al. (2023) was a subject of high uncertainty. However, the correspondence of the values with the eddy heat flux to the MIZ obtained in this study is striking.

The combination of the intensive eddy activity and high temperature gradients in the northern Greenland Sea makes this area specific for the Arctic. The EGC is a source of strong dynamic instability, which makes the study area to have the highest eddy kinetic energy in the Arctic (Wang et al., 2020). With this mechanism of horizontal mixing, the efficiency of eddy effect on the ice edge strongly depends on the horizontal variation of the SST in the MIZ and of eddy dynamic activity. Fixing temperature under the ice at the sea-water freezing point of −1.9°C, we can evaluate the SST variation by accessing the maximum SST in the MIZ, estimated within the 50 km distance from the ice edge. In the northern Greenland Sea and the Fram Strait the maximum SST in the MIZ, as defined above, decrease from 2—4°C at 77–80°N to −1—0°C at 70–75°N. The latter values are typical for the MIZ regions for other Eurasian Arctic seas during the warm period, except for the Barents Sea, where the maximum SST in the MIZ may reach 1°C. Thus, we can speculate that the effect on the ice edge of horizontal mixing by eddies in the study region would be stronger compared to most other MIZ regions in the Arctic.

Other high frequency processes also affect the ice edge. The effect of tides was investigated using high-resolution climate models with and without barotropic tides (Luneva et al., 2015; Schulz et al., 2025). In winter, the overall effect of tides is to decrease sea-ice concentration and thickness along the EGC in the annual mean by around 10% in the MIZ area of the EGC (Schulz et al., 2025). Overall, the increase in the heat flux from ocean to ice is 5%–10% of its mean value, resulting from an enhanced vertical exchange with the warmer Atlantic water below (Luneva et al., 2015). In summer, as increased mixing transports more heat from the mixed layer into the deeper ocean, this effect becomes less pronounced and may, in some regions, lead to an increase in sea-ice concentration and expansion of the ice-covered area.

High-frequency internal waves could be also generated within the MIZ or near the ice edge by winds blowing off the ice (Muench et al., 1983; Wadhams, 1983), due to tide-topography interactions (Padman & Dillon, 1991) or by ice keels drifting over a sharp elevated pycnocline (Eckert & Foster, 1990; Sandven & Johannessen, 1987; Zhang et al., 2022). In the first case, it leads to formation of distinct ice bands accumulated in the surface convergence zones promoting more rapid ice melting within these bands. The overall effect of internal waves propagating under the ice would be to enhance the turbulent dissipation rates and associated heat fluxes (Carr et al., 2019; Czipott et al., 1991; Padman & Dillon, 1991; Zhang et al., 2022). However, as patterns of internal waves are rather intermittent in the study region (Kozlov et al., 2024), accurate quantification of their net effect on sea ice retreat is rather challenging and needs dedicated field, laboratory or numerical experiments.

## Conflict of Interest

The authors declare no conflicts of interest relevant to this study.

## Data Availability Statement

The code of FESOM1.4, used in this study, is available at: https://doi.org/10.5281/zenodo.1116851. Daily sea-ice concentration data from AMSR-E microwave satellite are available from https://data.seaice.uni-bremen.de/amsre/.

**Acknowledgments**
The model analysis of sea-ice retreat by eddies in the marginal ice zone was funded by RSF project 25-17-00309, https://rscf.ru/project/25-17-00309/. W.Z. is supported by the National Natural Science Foundation of China (42576271; 42076225) and by the Fundamental Research Funds for the Central Universities (202562001).

## References

Alekseev, G. V., Johannessen, O. M., Korablev, A. A., Ivanov, V. V., & Kovalevsky, D. V. (2001). Interannual variability in water masses in the Greenland Sea and adjacent areas. *Polar Research*, *20*(2), 201–208. https://doi.org/10.3402/polar.v20i2.6518

Atadzhanova, O. A., Zimin, A. V., Romanenkov, D. A., & Kozlov, I. E. (2017). Satellite radar observations of small eddies in the White, Barents and Kara Seas. *Physical Oceanography*, *2*, 75–83. https://doi.org/10.22449/1573-160X-2017-2-75-83

Bashmachnikov, I., Belonenko, T. V., Kuibin, P. A., Volkov, D., & Foux, V. R. (2018). Patterns of vertical velocity of the Lofoten vortex (the Norwegian Sea). *Ocean Dynamics*, *68*(12), 1711–1725. https://doi.org/10.1007/s10236-018-1213-1

Bashmachnikov, I., & Carton, X. (2012). Surface signature of Mediterranean water eddies in the Northeastern Atlantic: Effect of the upper ocean stratification. *Ocean Science*, *8*(6), 931–943. https://doi.org/10.5194/os-8-931-2012

Bashmachnikov, I. L., Fedorov, A. M., Golubkin, P. A., Vesman, A. V., Selyuzhenok, V. V., Gnatiuk, N. V., et al. (2021). Mechanisms of interannual variability of deep convection in the Greenland Sea. *Deep-Sea Res. I Oceanogr. Res. Pap.*, *174*, 103557–103575. https://doi.org/10.1016/j.dsr.2021.103557

Bashmachnikov, I. L., Kozlov, I. E., Petrenko, L. A., Glok, N. I., & Wekerle, C. (2020). Eddies in the North Greenland Sea and Fram Strait from satellite altimetry, SAR and high-resolution model data. *J. Geophys. Res.-Oceans*, *125*(7), e2019JC015832. https://doi.org/10.1029/2019JC015832

Bashmachnikov, I. L., Raj, R. P., Golubkin, P., & Kozlov, I. E. (2023). Heat transport by mesoscale eddies in the Norwegian and Greenland seas. *Journal of Geophysical Research: Oceans*, *128*(2), e2022JC018987. https://doi.org/10.1029/2022JC018987

Bashmachnikov, I. L., Sokolovskiy, M. A., Belonenko, T. V., Volkov, D. L., Isachsen, P. E., & Carton, X. (2017). On the vertical structure and stability of the Lofoten vortex in the Norwegian Sea. *Deep-Sea Res. I Oceanogr. Res. Pap.*, *128*, 1–27. https://doi.org/10.1016/j.dsr.2017.08.001

Bondevik, E. (2011). Studies of eddies in the marginal ice Zone along the East Greenland Current using spaceborne Synthetic Aperture Radar (SAR). Master's thesis. *The University of Bergen*.

Bourke, R. H., Tunnicliffe, M. D., Newton, J. L., Paquette, R. G., & Manley, T. O. (1987). Eddy near the Molloy Deep revisited. *Journal of Geophysical Research*, *92*(C7), 6773–6776. https://doi.org/10.1029/JC092iC07p06773

Boyd, T. J., & D'Asaro, E. A. (1994). Cooling of the West Spitsbergen Current: Wintertime observations west of Svalbard. *Journal of Geophysical Research*, *99*(C11), 22597–22618. https://doi.org/10.1029/94JC01824

Buckley, M. W., & Marshall, J. (2016). Observations, inferences, and mechanisms of Atlantic meridional overturning circulation variability: A review. *Reviews of Geophysics*, *54*(1), 5–63. https://doi.org/10.1002/2015RG000493

Carr, M., Sutherland, P., Haase, A., Evers, K.-U., Fer, I., Jensen, A., et al. (2019). Laboratory experiments on internal solitary waves in ice-covered waters. *Geophysical Research Letters*, *46*(21), 12230–12238. https://doi.org/10.1029/2019GL084710

Comiso, J. C., Wadhams, P., Pedersen, L. T., & Gersten, R. A. (2001). Seasonal and interannual variability of the Odden ice tongue and a study of environmental effects. *Journal of Geophysical Research*, *106*(C5), 9093–9116. https://doi.org/10.1029/2000JC000204

Czipott, P. V., Levine, M. D., Paulson, C. A., Menemenlis, D., Farmer, D. M., & Williams, R. G. (1991). Ice flexure forced by internal wave packets in the Arctic Ocean. *Science*, *254*(5033), 832–835. https://doi.org/10.1126/science.254.5033.832

Danilov, S., Kivman, G., & Schröter, J. (2004). A finite-element ocean model: Principles and evaluation. *Ocean Modelling*, *6*(2), 125–150. https://doi.org/10.1016/S1463-5003(02)00063-X

Dokken, S. T., & Wahl, T. (1996). Observations of spiral eddies along the Norwegian coast in ERS SAR images. *Norwegian Defence Research Establishment (NDRE), Kjeller, Norway, Rep. 96/01463*, 29.

Dukhovskoy, D. S., Yashayaev, I., Proshutinsky, A., Bamber, J. L., Bashmachnikov, I. L., Chassignet, E. P., et al. (2019). Role of Greenland freshwater anomaly in the recent freshening of the subpolar North Atlantic. *J. Geophys. Res.-Oceans*, *124*(5), 3333–3360. https://doi.org/10.1029/2018JC014686

Eckert, E. G., & Foster, T. D. (1990). Upper ocean internal waves in the marginal ice zone of the northeastern Greenland Sea. *Journal of Geophysical Research*, *95*(C6), 9569–9574. https://doi.org/10.1029/JC095iC06p09569

Espedal, H. A., Johannessen, O. M., Johannessen, J. A., Dano, E., Lyzenga, D. R., & Knulst, J. C. (1998). COASTWATCH'95: ERS 1/2 SAR detection of natural film on the ocean surface. *Journal of Geophysical Research*, *103*(C11), 24969–24982. https://doi.org/10.1029/98JC01660

Fine, E. C., MacKinnon, J. A., Alford, M. H., & Mickett, J. B. (2018). Microstructure observations of turbulent heat fluxes in a warm-core Canada Basin eddy. *Journal of Physical Oceanography*, *48*(10), 2397–2418. https://doi.org/10.1175/JPO-D-18-0028.1

Germe, A., Houssais, M. N., Herbaut, C., & Cassou, C. (2011). Greenland Sea sea ice variability over 1979-2007 and its link to the surface atmosphere. *Journal of Geophysical Research*, *116*(C10), 1–14. https://doi.org/10.1029/2011JC006960

Glessmer, M. S., Eldevik, T., Våge, K., Nilsen, J. E. Ø., & Behrens, E. (2014). Atlantic origin of observed and modelled freshwater anomalies in the Nordic Seas. *Nature Geoscience*, *7*(11), 801–805. https://doi.org/10.1038/ngeo2259

Gupta, M., Marshall, J., Song, H., Campin, J. M., & Meneghello, G. (2020). Sea-ice melt driven by ice-ocean stresses on the mesoscale. *J. Geophys. Res.-Oceans*, *125*(11), 1–20. https://doi.org/10.1029/2020JC016404

Gupta, M., & Thompson, A. F. (2022). Regimes of sea-ice floe melt: Ice-ocean coupling at the submesoscales. *J. Geophys. Res.-Oceans*, *127*(9), e2022JC018894. https://doi.org/10.1029/2022JC018894

Haak, H., Jungclaus, J., Mikolajewicz, U., & Latif, M. (2003). Formation and propagation of great salinity anomalies. *Geophysical Research Letters*, *30*(9), 1–4. https://doi.org/10.1029/2003GL017065

Häkkinen, S. (1986). Coupled ice-ocean dynamics in the marginal ice zones: Upwelling/downwelling and eddy generation. *Journal of Geophysical Research*, *91*(C1), 819–832. https://doi.org/10.1029/JC091iC01p00819

Hattermann, T., Isachsen, P. E., von Appen, W. J., Albretsen, J., & Sundfjord, A. (2016). Eddy-driven recirculation of Atlantic Water in Fram Strait. *Geophysical Research Letters*, *43*(7), 3406–3414. https://doi.org/10.1002/2016GL068323

Hibler, W. D. (1984). Ice dynamics. No. CRRELMONO843.

Hunke, E. C., & Dukowicz, J. K. (2002). The elastic–viscous–plastic sea ice dynamics model in general orthogonal curvilinear coordinates on a sphere—Incorporation of metric terms. *Monthly Weather Review*, *130*(7), 1848–1865. https://doi.org/10.1175/1520-0493(2002)130<1848:TEVPSI>2.0.CO;2

Johannessen, J. A., Johannessen, O. M., Svendsen, E., Shuchman, R., Manley, T., Campbell, W. J., et al. (1987). Mesoscale eddies in the Fram Strait marginal ice zone during the 1983 and 1984 Marginal Ice Zone experiments. *Journal of Geophysical Research*, *92*(C7), 6754–6772. https://doi.org/10.1029/JC092iC07p06754

Johannessen, J. A., Shuchman, R. A., Digranes, G., Lyzenga, D. R., Wackerman, C., Johannessen, O. M., & Vachon, P. W. (1996). Coastal ocean fronts and eddies imaged with ERS 1 synthetic aperture radar. *Journal of Geophysical Research*, *101*(C3), 6651–6667. https://doi.org/10.1029/95JC02962

Johannessen, O. M., Johannessen, J. A., Svendsen, E., Shuchman, R. A., Campbell, W. J., & Josberger, E. (1987). Ice-edge eddies in the Fram Strait marginal ice zone. *Science*, *236*(4800), 427–429. https://doi.org/10.1126/science.236.4800.427

Kaledina, A. S., & Bashmachnikov, I. L. (2023). Characteristics of density inversions in the Greenland Sea during the cold seasons of 1993-2019. *Physical Oceanography*, *30*, 18–26. https://doi.org/10.29039/1573-160X-2023-1-18-26

Karimova, S. S. (2012). Spiral eddies in the Baltic, Black and Caspian seas as seen by satellite radar data. *Advances in Space Research*, *50*(8), 1107–1124. https://doi.org/10.1016/j.asr.2011.10.027

Karimova, S. S., & Gade, M. (2016). Improved statistics of sub-mesoscale eddies in the Baltic Sea retrieved from SAR imagery. *International Journal of Remote Sensing*, *37*(10), 2394–2414. https://doi.org/10.1080/01431161.2016.1145367

Kolas, E., & Fer, I. (2018). Hydrography, transport and mixing of the West Spitsbergen Current: The Svalbard Branch in summer 2015. *Ocean Science*, *14*(6), 1603–1618. https://doi.org/10.5194/os-14-1603-2018

Kozlov, I. E., Artamonova, A. V., Manucharyan, G. E., & Kubryakov, A. A. (2019). Eddies in the Western Arctic Ocean from spaceborne SAR observations over open ocean and marginal ice zones. *J. Geophys. Res.-Oceans*, *124*(9), 6601–6616. https://doi.org/10.1029/2019JC015113

Kozlov, I. E., & Atadzhanova, O. A. (2022). Eddies in the marginal ice zone of Fram Strait and Svalbard from spaceborne SAR observations in winter. *Remote Sensing*, *14*, 1–19. https://doi.org/10.3390/rs14010134

Kozlov, I. E., Kudryavtsev, V. N., Johannessen, J. A., Chapron, B., Dailidiene, I., & Myasoedov, A. G. (2012). ASAR imaging for coastal upwelling in the Baltic Sea. *Advances in Space Research*, *50*(8), 1125–1137. https://doi.org/10.1016/j.asr.2011.08.017

Kozlov, I. E., Mikhaylichenko, T. V., & Petrenko, L. A. (2024). Properties of short-period internal waves near Svalbard from Sentinel-1 satellite data. *Russian Journal of Earth Sciences*, *24*, ES5008. https://doi.org/10.2205/2024ES000951

Kozlov, I. E., Plotnikov, E. V., & Manucharyan, G. E. (2020). Brief communication: Mesoscale and submesoscale dynamics in the marginal ice zone from sequential synthetic aperture radar observations. *The Cryosphere*, *14*(9), 2941–2947. https://doi.org/10.5194/tc-14-2941-2020

Kwok, R. (2004). Annual cycles of multiyear sea ice coverage of the Arctic Ocean: 1999–2003. *Journal of Geophysical Research*, *109*(C11), 1–13. https://doi.org/10.1029/2003JC002238

Kwok, R., Cunningham, G. F., & Pang, S. S. (2004). Fram Strait sea ice outflow. *Journal of Geophysical Research*, *109*(C1), 1–14. https://doi.org/10.1029/2003JC001785

Kwok, R., Cunningham, G. F., Wensnahan, M., Rigor, I., Zwally, H. J., & Yi, D. (2009). Thinning and volume loss of the Arctic Ocean sea ice cover: 2003-2008. *Journal of Geophysical Research*, *114*(C7), 1–16. https://doi.org/10.1029/2009JC005312

Large, W., & Yeager, S. (2008). The global climatology of an interannually varying air-sea flux data set. *Climate Dynamics*, *33*(2–3), 341–364. https://doi.org/10.1007/s00382-008-0441-3

Luneva, M. V., Aksenov, Y., Harle, J. D., & Holt, J. T. (2015). The effects of tides on the water mass mixing and sea-ice in the Arctic Ocean. *J. Geophys. Res.-Oceans*, *120*(10), 6669–6699. https://doi.org/10.1002/2014JC010310

Manley, T. O. (1987). Effects of sub-ice mesoscale features within the marginal ice zone of Fram Strait. *Journal of Geophysical Research*, *92*(C4), 3944–3960. https://doi.org/10.1029/JC092iC04p03944

Manucharyan, G. E., & Thompson, A. F. (2017). Submesoscale sea ice-ocean interactions in marginal ice zones. *J. Geophys. Res.-Oceans*, *122*(12), 9455–9475. https://doi.org/10.1002/2017JC012895

Manucharyan, G. E., & Thompson, A. F. (2022). Heavy footprints of upper-ocean eddies on weakened Arctic sea ice in marginal ice zones. *Nature Communications*, *13*(1), 2147. https://doi.org/10.1038/s41467-022-29663-0

Manucharyan, G. E., & Timmermans, M. L. (2013). Generation and separation of mesoscale eddies from surface ocean fronts. *Journal of Physical Oceanography*, *43*(12), 2545–2562. https://doi.org/10.1175/JPO-D-13-094.1

Marshall, J., Kushnir, Y., Battisti, D., Chang, P., Czaja, A., Dickson, R., et al. (2001). North Atlantic climate variability: Phenomena, impacts and mechanisms. *International Journal of Climatology*, *21*(15), 1863–1898. https://doi.org/10.1002/joc.693

Meincke, J., Jonsson, S., & Swift, J. H. (1992). Variability of convective conditions in the Greenland Sea, ICES mar. *Sci. Symp.*, *195*, 32–39. https://doi.org/10.17895/ices.pub.19270616

Meneghello, G., Marshall, J., Campin, J. M., Doddridge, E., & Timmermans, M. L. (2018). The ice-ocean governor: Ice-ocean stress feedback limits Beaufort Gyre spin-up. *Geophysical Research Letters*, *45*(20), 11293–11299. https://doi.org/10.1029/2018GL080171

Mensa, J. A., Timmermans, M. L., Kozlov, I. E., Williams, W. J., & Özgökmen, T. M. (2018). Surface drifter observations from the Arctic Ocean's Beaufort Sea: Evidence for submesoscale dynamics. *J. Geophys. Res.-Oceans*, *123*(4), 2635–2645. https://doi.org/10.1002/2017JC013728

Mironov, E. U. (Ed.) (2004). *Ice conditions in the Greenland and Barents Seas and their long-term forecast* (p. 320). AARI Publishing. (in Russian).

Morozov, E. A., & Kozlov, I. E. (2023). Eddies in the Arctic Ocean revealed from MODIS optical imagery. *Remote Sensing*, *15*(6), 1–23. https://doi.org/10.3390/rs15061608

Muench, R. D., LeBlond, P. H., & Hachmeister, L. E. (1983). On some possible interactions between internal waves and sea ice in the marginal ice zone. *Journal of Geophysical Research*, *88*(C5), 2819–2826. https://doi.org/10.1029/JC088iC05p02819

Munk, W., Armi, L., Fischer, K., & Zachariasen, F. (2000). Spirals on the sea. *Proceedings of the Royal Society of London A.*, *456*(1997), 1217–1280. https://doi.org/10.1098/rspa.2000.0560

Nencioli, F., Dong, C., Dickey, T., Washburn, L., & McWilliams, J. C. (2010). A Vector geometry-based Eddy detection Algorithm and its application to a high-resolution numerical model product and high-frequency radar surface velocities in the Southern California bight. *Journal of Atmospheric and Oceanic Technology*, *27*(3), 564–579. https://doi.org/10.1175/2009JTECHO725.1

Nilsen, F., Gjevik, B., & Schauer, U. (2006). Cooling of the West Spitsbergen Current: Isopycnal diffusion by topographic vorticity waves. *Journal of Geophysical Research*, *111*(C8), 1–16. https://doi.org/10.1029/2005JC002991

Padman, L., & Dillon, T. M. (1991). Turbulent mixing near the yermak Plateau during the coordinated Eastern Arctic experiment. *Journal of Geophysical Research*, *96*(C3), 4769–4782. https://doi.org/10.1029/90JC02260

Parkinson, C. L., Cavalieri, D. J., Gloersen, P., Zwally, H. J., & Comiso, J. C. (1999). Arctic sea ice extents, areas, and trends, 1978-1996. *Journal of Geophysical Research*, *104*(C9), 20837–20856. https://doi.org/10.1029/1999JC900082

Parkinson, C. L., & Washington, W. M. (1979). A large-scale numerical model of sea ice. *Journal of Geophysical Research*, *84*(C1), 311–337. https://doi.org/10.1029/JC084iC01p00311

Perovich, D. K., Tucker III, W. B., & Krishfield, R. A. (1989). Oceanic heat flux in the Fram Strait measured by a drifting buoy. *Geophysical Research Letters*, *16*(9), 995–998. https://doi.org/10.1029/GL016i009p00995

Peterson, B. J., McClelland, J., Curry, R., Holmes, R. M., Walsh, J. E., & Aagaard, K. (2006). Trajectory shifts in the Arctic and subarctic freshwater cycle. *Science*, *313*(5790), 1061–1066. https://doi.org/10.1126/science.1122593

Petrenko, L. A., & Kozlov, I. E. (2021). Eddy generation and variability of the marginal ice zone in the Fram Strait according to satellite radar measurements. *Journal of Physics: Conf., 2057*, *2057*, 1–6. https://doi.org/10.1088/1742-6596/2057/1/012022

Petrenko, L. A., & Kozlov, I. E. (2023). Variability of the marginal ice Zone and eddy generation in fram Strait and near Svalbard in summer based on satellite radar observations. *Physical Oceanography*, *30*(5), 594–611.

Pnyushkov, A., Polyakov, I. V., Padman, L., & Nguyen, A. T. (2018). Structure and dynamics of mesoscale eddies over the Laptev Sea continental slope in the Arctic Ocean. *Ocean Science*, *14*(5), 1329–1347. https://doi.org/10.5194/os-14-1329-2018

Rhein, M., Kieke, D., Hüttl-Kabus, S., Roessler, A., Mertens, C., Meissner, R., et al. (2011). Deep water formation, the subpolar gyre, and the meridional overturning circulation in the subpolar North Atlantic. *Deep-Sea Res. II Top. Stud. Oceanogr.*, *58*, 1819–1832. https://doi.org/10.1016/j.dsr2.2010.10.061

Ricker, R., Girard-Ardhuin, F., Krumpen, T., & Lique, C. (2018). Satellite-derived sea ice export and its impact on Arctic ice mass balance. *The Cryosphere*, *12*(9), 3017–3032. https://doi.org/10.5194/tc-12-3017-2018

Rogers, J. C., & Hung, M. P. (2008). The Odden ice feature of the Greenland Sea and its association with atmospheric pressure, wind, and surface flux variability from reanalyses. *Geophysical Research Letters*, *35*(8), 1–5. https://doi.org/10.1029/2007GL032938

Rudels, B., Korhonen, M., Budéus, G., Beszczynska-Möller, A., Schauer, U., Nummelin, A., et al. (2012). The East Greenland Current and its impacts on the Nordic Seas: Observed trends in the past decade. *ICES Journal of Marine Science*, *69*, 841–851. https://doi.org/10.1093/icesjms/fss079

Sandven, S., & Johannessen, O. M. (1987). High-frequency internal wave observations in the marginal ice zone. *Journal of Geophysical Research*, *92*(C7), 6911–6920. https://doi.org/10.1029/JC092iC07p06911

Sandven, S., Johannessen, O. M., & Johannessen, J. A. (1991). Mesoscale eddies and chimneys in the marginal ice zone. *Journal of Marine Systems*, *2*(1–2), 195–208. https://doi.org/10.1016/0924-7963(91)90024-O

Schulz, K., Nguyen, A. T., Pillar, H. R., Baumann, T. M., Muilwijk, M., Fer, I., et al. (2025). Quantifying tidal impacts on Arctic sea ice: An unexpected mechanism for the regional delay of summer melting. *Journal of Physical Oceanography*, *55*(11), 1951–1970. https://doi.org/10.1175/JPO-D-24-0255.1

Selyuzhenok, V., Bashmachnikov, I., Ricker, R., Vesman, A., & Bobylev, L. (2020). Sea ice volume variability and water temperature in the Greenland Sea. *The Cryosphere*, *14*(2), 477–495. https://doi.org/10.5194/tc-14-477-2020

Serreze, M. C., Barrett, A. P., Slater, A. G., Woodgate, R. A., Aagaard, K., Lammers, R. B., et al. (2006). The large-scale freshwater cycle of the Arctic. *Journal of Geophysical Research*, *111*(C11), 1–19. https://doi.org/10.1029/2005JC003424

Shalina, E. V. (2021). Regional variability of sea-ice in the Russian Arctic and on the Northern Sea Route observed from satellites. *Sovremennye problemy distantsionnogo zondirovaniya Zemli iz kosmosa*, *18*(5), 201–213. (in Russian). https://doi.org/10.21046/2070-7401-2021-18-5-201-213

Shuchman, R. A., Josberger, E. G., Russel, C. A., Fischer, K. W., Johannessen, O. M., Johannessen, J., & Gloersen, P. (1998). Greenland Sea Odden sea ice feature: Intra-annual and interannual variability. *Journal of Geophysical Research*, *103*(C6), 12709–12724. https://doi.org/10.1029/98JC00375

Smedsrud, L. H., Halvorsen, M. H., Stroeve, J. C., Zhang, R., & Kloster, K. (2017). Fram Strait sea ice export variability and September Arctic sea-ice extent over the last 80 years. *The Cryosphere*, *11*(1), 65–79. https://doi.org/10.5194/tc-11-65-2017

Smith, D. C., IV, & Bird, A. A. (1991). The interaction of an ocean eddy with an ice edge ocean jet in a marginal ice zone. *Journal of Geophysical Research*, *96*(C3), 4675–4689. https://doi.org/10.1029/90JC02262

Spall, M. A., Pickart, R. S., Fratantoni, P. S., & Plueddemann, A. J. (2008). Western arctic shelfbreak eddies: Formation and transport. *Journal of Physical Oceanography*, *38*(8), 1644–1668. https://doi.org/10.1175/2007JPO3829.1

Spreen, G., Kaleschke, L., & Heygster, G. (2008). Sea ice remote sensing using AMSR-E 89-GHz channels. *Journal of Geophysical Research*, *113*(C2), 1–14. https://doi.org/10.1029/2005JC003384

Timmermann, R., Danilov, S., Schröter, J., Böning, C., Sidorenko, D., & Rollenhagen, K. (2009). Ocean circulation and sea-ice distribution in a finite element global sea ice-ocean model. *Ocean Modelling*, *27*, 114–129. https://doi.org/10.1016/j.ocemod.2008.10.009

Trodahl, M., & Isachsen, P. E. (2018). Topographic influence on baroclinic instability and the mesoscale Eddy field in the Northern North Atlantic Ocean and the nordic Seas. *Journal of Physical Oceanography*, *48*(11), 2593–2607. https://doi.org/10.1175/JPO-D-17-0220.1

Vinje, T., & Finnekåsa, Ø. (1986). The ice transport through the Fram Strait, Skr. *Norsk Polarinst.*, *186*(39).

Visbeck, M., Fischer, J., & Schott, F. (1995). Preconditioning the Greenland Sea for deep convection: Ice formation and ice drift. *Journal of Geophysical Research*, *100*(C9), 18489–18502. https://doi.org/10.1029/95JC01611

von Appen, W. J., Schauer, U., Somavilla, R., Bauerfeind, E., & Beszczynska-Möller, A. (2015). Exchange of warming deep waters across Fram Strait. *Deep-Sea Res. I Oceanogr. Res. Pap.*, *103*, 86–100. https://doi.org/10.1016/j.dsr.2015.06.003

von Appen, W. J., Wekerle, C., Hehemann, L., Schourup-Kristensen, V., Konrad, C., & Iversen, M. H. (2018). Observations of a submesoscale cyclonic filament in the marginal ice Zone. *Geophysical Research Letters*, *45*(12), 6141–6149. https://doi.org/10.1029/2018GL077897

von Appen, W. J. V., Schauer, U., Hattermann, T., & Beszczynska-Möller, A. (2016). Seasonal cycle of mesoscale instability of the West Spitsbergen Current. *Journal of Physical Oceanography*, *46*(4), 1231–1254. https://doi.org/10.1175/JPO-D-15-0184.1

Wadhams, P. (1983). A mechanism for the formation of ice edge bands. *Journal of Geophysical Research*, *88*(C05), 2813–2818. https://doi.org/10.1029/JC088iC05p02813

Wadhams, P., Comiso, J. C., Prussen, E., Wells, S., Brandon, M., Aldworth, E., et al. (1996). The development of the Odden ice tongue in the Greenland Sea during winter 1993 from remote sensing and field observations. *J. Geophys. Res.Ocean*, *101*(C8), 18213–18235. https://doi.org/10.1029/96JC01440

Wadhams, P., & Squire, V. A. (1983). An ice-water vortex at the edge of the East Greenland Current. *Journal of Geophysical Research*, *88*(C5), 2770–2780. https://doi.org/10.1029/JC088iC05p02770

Wang, Q., Koldunov, N. V., Danilov, S., Sidorenko, D., Wekerle, C., Scholz, P., et al. (2020). Eddy kinetic energy in the Arctic Ocean from a global simulation with a 1-km Arctic. *Geophysical Research Letters*, *47*(14), e2020GL088550. https://doi.org/10.1029/2020GL088550

Watkins, D. M., Bliss, A. C., Hutchings, J. K., & Wilhelmus, M. M. (2023). Evidence of abrupt transitions between Sea ice dynamical regimes in the East Greenland marginal ice Zone. *Geophysical Research Letters*, *50*(15), 1–10. https://doi.org/10.1029/2023GL103558

Wekerle, C. (2013). *Dynamics of the Canadian Arctic Archipelago throughflow: A numerical study with a finite element sea-ice and ocean model*. PhD thesis. University of Bremen. Retrieved from https://nbn-resolving.de/urn:nbn:de:gbv:46-00103421-10

Wekerle, C., Hattermann, T., Wang, Q., Crews, L., von Appen, W. J., & Danilov, S. (2020). Properties and dynamics of mesoscale eddies in Fram Strait from a comparison between two high-resolution ocean–sea-ice models. *Ocean Science*, *16*(5), 1225–1246. https://doi.org/10.5194/os-16-1225-2020

Wekerle, C., Wang, Q., von Appen, W. J., Danilov, S., Schourup-Kristensen, V., & Jung, T. (2017). Eddy-resolving simulation of the Atlantic water circulation in the Fram Strait with focus on the seasonal cycle. *J. Geophys. Res.Ocean*, *122*(11), 8385–8405. https://doi.org/10.1002/2017JC012974

Widell, K., Østerhus, S., & Gammelsrød, T. (2003). Sea ice velocity in the Fram Strait monitored by moored instruments. *Geophysical Research Letters*, *30*, 1–4. https://doi.org/10.1029/2003GL018119

Zhang, P., Li, Q., Xu, Z., & Yin, B. (2022). Internal solitary wave generation by the tidal flows beneath ice keel in the Arctic Ocean. *Journal of Oceanology and Limnology*, *40*(3), 831–845. https://doi.org/10.1007/s00343-021-1052-7

Zhurbas, V., Väli, G., & Kuzmina, N. (2019). Rotation of floating particles in submesoscale cyclonic and anticyclonic eddies: A model study for the southeastern Baltic Sea. *Ocean Science*, *15*(6), 1691–1705. https://doi.org/10.5194/os-15-1691-2019